

1 **Original Article**

2 **The Neochord Mitral Valve Repair Procedure: Numerical Simulation of Different Neochords Tensioning**

3 **Protocols**

4 *Luigi Di Micco<sup>1</sup>, Paolo Peruzzo<sup>1</sup>, Andrea Colli<sup>2</sup>, Gaetano Burriesci<sup>3,4</sup>, Daniela Boso<sup>1</sup>, Laura Besola<sup>2</sup>, Gino*

5 *Gerosa<sup>2</sup> & Francesca M. Susin<sup>1</sup>*

6 1 Cardiovascular Fluid Dynamics Laboratory, ICEA Department, University of Padova, Italy;

7 2 DSCTV, University of Padova Medical School, Italy;

8 3 UCL Mechanical Engineering, University College London, United Kingdom;

9 4 Ri.MED Foundation, Palermo, Italy.

10

11 **Corresponding Author:**

12 Luigi Di Micco

13 Cardiovascular Fluid Dynamics Laboratory, ICEA Department

14 University of Padova, Italy

15 Via Loredan 20, 35131 Padova (Italy)

16 phone: +39 049 827 5433

17 e-mail: [luigi.dimicco@dicea.unipd.it](mailto:luigi.dimicco@dicea.unipd.it)

18 **Word count:** 3421

19

20 **Keywords:** NeoChord procedure, Mitral Valve Repair, Finite Elements Analysis, Tensioning Strategies, Mitral

21 Valve Prolapse,

22

23 **ABSTRACT**

24 Transapical off-pump mitral valve repair with neochord implantation is an established technique for  
25 minimally-invasive intervention on mitral valve prolapse/flail. The procedure involves the positioning of  
26 artificial chords, whose length/tension is adjusted intraoperatively, adopting different methods based on  
27 the experience of the surgeon. This unsystematic approach occasionally leads to complications such as  
28 leaflet rupture and excessive/insufficient load on the neochords. In this study, finite element models of a  
29 generalized prolapsing mitral valve are used to verify the effect of two alternative tensioning approaches  
30 (AT – All together and 1by1 – one by one sequences) on the coaptation area and valve biomechanics,  
31 comparing results with a corresponding healthy configuration. The total force of about 1 N is exerted by the  
32 chords in both strategies, but the maximum stress and coaptation area are closer to those of the healthy  
33 configuration in the 1by1 sequence. However, the analysis also provides an explanation for the chords  
34 unloading in the 1by1 strategy observed in the clinical practice, and suggests an optimum tensioning  
35 methodology for NeoChord procedures. The study also reveals the potential power of the implemented  
36 numerical approach to serve as a tool for procedural planning, supporting the identification of the most  
37 suitable ventricular access site and the most effective stitching points for the artificial chords.

38 **INTRODUCTION**

39 Experimental and numerical investigations are nowadays largely used to assess the safety and efficacy of  
40 cardiovascular devices and procedures, by identifying an enhanced medical practice and support clinical  
41 decisions [1]–[6]. However, the application of these approaches to treatments of mitral valve (MV) diseases  
42 still represents a major challenge, due to the complex anatomy of the valvular and subvalvular apparatus.

43 Mitral regurgitation (MR) is one of the most complex valvular diseases. MR is classified into two categories:  
44 functional MR (FMR), due to left ventricular (LV) dilation and dysfunction, and degenerative MR (DMR), due  
45 to a structural abnormality of the valve apparatus, mainly. The latter can lead, among possible valve  
46 failures, to prolapse or flail [7]–[9]. Recently a new MV procedure with off-pump transcatheter access with  
47 neochord implantation has emerged as a new promising surgical procedure to restore the functionality of  
48 DMR [10], [11]. It consists in the replacement of native chordae tendineae with artificial tethers, inserted

49 by transapical access. The clinical outcome has confirmed the safety and effectiveness of the approach [12],  
50 enlightening the issues to be addressed to enhance the reliability of the procedure and support  
51 preoperative planning. In particular, the optimum tensioning of the artificial chords still needs to be  
52 determined, in order to maximize the efficacy of the technique and the durability of the solution [13]. This  
53 issue is further complicated by the fact that the transapical implantation approach results in non-  
54 physiological orientations of the artificial sutures, which load the leaflet along directions different from the  
55 native chordae

56 A number of in vitro and in silico studies have attempted to study the biomechanics of MV repair with neo-  
57 chords implantation [14]–[19] analysing the post-implant configuration after the complete surgical  
58 procedure. Differently by the cited studies, the NeoChord procedure is performed in beating-heart.  
59 Consequently, in order to identify the most suitable implantation protocol and the commonly reported  
60 procedural complications, such as leaflet rupture or neochords overloading/unloading, the study of  
61 NeoChord procedure also requires the investigation of the leaflet coaptation and stress pattern during the  
62 chords positioning, i.e. during the operative phase of the implant procedure. Recently, a FEM analysis was  
63 developed in order to evaluate the sutures length effect in MV repair with transapical neochord  
64 implantation [20]. However, the main focus of our present study consists in analysing the procedural and  
65 post-implant outcome of the two strategies currently in use for neochords tensioning during the repair:

- 66 • the *'all together'* strategy, i.e. all chords are tensioned contemporarily all together;
- 67 • the *'one by one'*, i.e. the chords are tensioned one at the time by subsequently applying to each  
68 chord a proper tensioning with a certain order.

69 For both tensioning strategies, the intraoperative behavior of leaflet coaptation, the stress distribution in  
70 the valve apparatus, and the tensioning force in each chord are determined by means of numerical  
71 simulations of a generalised MV prolapse.

## 72 METHODS

### 73 Mitral valve model

74 Healthy MV prevents blood backflow from the left ventricle to atrium during systole by coaptation of  
75 posterior and anterior leaflets; a number of tendinous strings (*chordae tendinae*) contribute to holding the  
76 closed valve in place, by tethering the leaflets to the ventricular wall via papillary muscles structure.  
77 Leaflets were designed to include the common anatomical segments usually identified, including the  
78 anterior leaflet scallop, *A*; the commissural leaflet scallops, *C1* and *C2*; the posterior leaflet scallops *P1*, *P2*,  
79 and *P3*, as represented in Figure 1. All main parameters of valve geometry, e.g. the thickness and cross-  
80 sectional area used for the leaflets and chordae in the various portions of the model, are summarized in  
81 Table 1.

82 Since the proposed study is concerned essentially with the systolic phase, the dynamic motion of the  
83 annulus and papillary muscles were not simulated, keeping the annular profile fixed on a plane and  
84 maintaining a constant distance between the annulus plane and the papillary muscles (idealized as  
85 anchoring points - red dots in Figure 1). These assumptions, which are common in the literature [21], [22],  
86 are considered acceptable due to the comparative nature of this study.

87 Leaflets were modeled as membranes, with the isotropic hyperelastic incompressible constitutive law  
88 based on a 5<sup>th</sup> order reduced polynomial strain energy potential formulation. According to previous works  
89 concerning the analysis of MV repair [23]–[26],  $U$  reads:

$$U = \sum_{i=1}^5 C_{i0} (\bar{I}_1 - 3)^i + \sum_{i=1}^5 \frac{1}{D_i} (J_{el} - 1)^{2i} \quad (1)$$

90

91 Where  $\bar{I}_1$  is the first deviatoric strain invariant  $\bar{I}_1 = \bar{\lambda}_1^2 + \bar{\lambda}_2^2 + \bar{\lambda}_3^2$ , where  $\bar{\lambda}_i = J^{-\frac{1}{3}} \lambda_i$  are the deviatoric  
92 stretches, with  $J$  the total volume ratio and  $\lambda_i$  the principal stretches;  $C_{i0}$  and  $D_i$  are the coefficients  
93 determined from mechanical tests performed on porcine mitral valves [27], averaging data obtained along  
94 radial and circumferential direction, and they are summarized in table 2. The anisotropy shown by the  
95 biaxial tensile tests performed by May-Newman appears rather reduced and, given the comparative

96 purpose of the present work, it was decided to assume an isotropic hyperelastic behavior for the leaflet's  
97 tissue.

98 Chords were modelled as linear elastic trusses, with Young modulus ( $E$ ) equal to 40 MPa (Kunzelman et al.,  
99 1996; Lau et al., 2010);

100 In the neochord procedure, artificial chords are usually obtained from e-PTFE *CV-4 Gore-Tex* sutures with a  
101 cross-section of  $0.074 \text{ mm}^2$ , tied to the leaflet margin with a girth hitch knot approach, resulting in two  
102 suture stands pulled in the same direction [29]. In the model, each artificial chord was represented by  
103 linear truss element with a circular cross-section of  $0.148 \text{ mm}^2$  (i.e. equal to the sum of the cross-section of  
104 the two stands). The neochord's Young modulus was determined experimentally by performing tension  
105 testing on an e-PTFE wire. For the test, the wire was settled on the tensile testing machine (Zwick-Roll,  
106 *Zwick GmbH & Co.KG, Zwick USA*) in a wet environment of saline solution at a temperature of  $37^\circ$ , to  
107 recreate physiological conditions. A 40 mm initial length was used, i.e. the length of the neochords in the  
108 numerical model. Results suggested a value of the Young modulus equal to 2.3 GPa for the *CV-4 Gore-Tex*  
109 *suture*.

## 110 **Simulations**

111 The mitral valve was modeled by using the explicit approach with the finite element code ABAQUS  
112 (SIMULIA, Providence, RI). Leaflets and chords were represented by linear triangular membrane elements  
113 (2D elements) and truss (1D elements), respectively. The connections between the leaflets free-margin and  
114 the chordae tendineae were modeled simulating the physiological intra-leaflets insertion of the native  
115 chords as described by Muresian (2009) ,[31], on the basis of an accurate clinical analysis. In the model,  
116 along with the free-margin insertion, the native chordae elements were prolonged inside the leaflets by  
117 sharing the same nodes discretization for three nodes, thus avoiding unrealistic stress concentration and  
118 singularity points.

119 The nodes describing the annulus were fixed in space, allowing rotations of the leaflets elements about all  
120 axes. Similarly, the chordae were pinned at the nodes corresponding to the papillary muscles. The unloaded  
121 valve model was generated in a fully open position [32].

122 The closed configuration was achieved by applying a spatially uniform pressure on the ventricular side.  
123 Since the model does not describe the annulus and papillary muscles dynamics occurring during the cardiac  
124 cycle, some preliminary simulations were performed to verify the effect of the load history on the systolic  
125 configuration. In particular, the comparison between the values of the maximum principal stresses at the  
126 peak load, which were obtained applying physiologically pulsatile pressures and steady pressure conditions  
127 reached by ramping the load linearly (Figure 2c), indicated lower stress in pulsatile condition, with  
128 differences inferior to 10%. Differences in term of displacement were negligible and inferior to 0.5%.  
129 Hence, the decision was taken to apply a spatially uniform pressure linearly increasing from 0 to 120 mmHg  
130 in 200 ms (corresponding to the systolic peak) to the ventricular side of the valve, for all analyzed cases.  
131 This approach significantly reduced the overall computational cost of the simulations, as well.

132 A reference model, including the presence and healthy function of all chordae, was run to estimate the  
133 optimal anterior-posterior leaflets coaptation achievable with the selected MV description (see Figure 1). A  
134 MV incompetence was then simulated by detaching six central chords (see green chords in Figure 1),  
135 leading to a central width prolapse (P2 section in Figure 2a) that is the most common leaflet disease for  
136 patients who underwent NeoChord repair [33].

137 In the prolapsed scenario, the repair was simulated by adding four artificial neochords between the margin  
138 of the prolapsed leaflets portion and the ventricle entry site (see Figure 2b), [34]. The entry site was located  
139 40 mm apart from the annulus, according to in-vivo measurements, to form the optimal neochord  
140 trajectory implantation [35].

141 In the first stage of the analysis, the four sutures were not tensioned until the maximum pressure load was  
142 achieved (case of implanted but inactive artificial chords to mimic the prolapsed pre-tensioning  
143 configuration) so that the valve reached the idealized prolapse condition before the tensioning. From the  
144 end-diastole configuration, with a linear pressure load from 0 to 120 mmHg, the valve is forced to close.  
145 During this first stage of the simulation, all the artificial sutures implanted were not tensioned (i.e. one side  
146 is attached to the leaflet while the other side was free to move in order to simulate the clinical phase

147 during which the external sutures remain outside the ventricle before the tensioning stage). In the second  
148 stage of the analysis, two different strategies for restoring the valve coaptation were pursued. In the first  
149 one, indicated as *all together* strategy (AT) the four chords were tensioned contemporarily, by applying the  
150 displacement required to restore leaflets coaptation (Figure 3a). In the second strategy, indicated as *one by*  
151 *one* strategy (1by1), the four chords were tensioned one at the time by subsequently applying to each  
152 chord the same displacement as the AT case. In all simulations, for all the schemes analyzed, the tensioning  
153 was performed by imposing at the proximal nodes of the artificial sutures the same outward displacement  
154 along the longitudinal direction. Such displacement promotes the reduction of the prolapsed portion of the  
155 posterior leaflet, since its margin moves towards the anterior one, until the repaired configuration is  
156 achieved. The prescribed displacement was set equal to 11 mm, to obtain the proper coaptation length.  
157 This value was defined after some preliminary analysis by tuning the chords displacement until the  
158 maximum coaptation length between the anterior and posterior free margin was measured at the anterior-  
159 posterior axis (see Figure 1). In order to compare the two pulling strategies, we chose to prescribe the same  
160 displacement of the sutures in all simulations, coherently with the clinical practice, where clinicians can  
161 easily control the chordae displacement. In order to examine the different strategies commonly adopted by  
162 surgeons when repairing MV prolapse by NeoChord procedure, the following possible sequences of chord  
163 pulling were simulated (figure 3b):

- 164 a) central to lateral pulling (1by1a);
- 165 b) lateral to central (1by1b);
- 166 c) lateral to lateral (1by1c).

## 167 **RESULTS**

168 The healthy configuration of the generalized MV model produced a leaflets coaptation length along the axis  
169 of symmetry of about 8 mm, corresponding to a total contact area,  $A_{c,H}$ , between the anterior and posterior  
170 leaflet of about 270 mm<sup>2</sup>. The contact area,  $A_c$ , restored during neochords tensioning procedures,  
171 normalized with  $A_{c,H}$  is reported in Figure 4.

172 Figure 5 shows the contour map of the stress field computed on the treated leaflet  $P2$  for all analyzed  
173 configurations. A scale from 0 to 0.5 MPa was chosen to better visualize the areas of stress concentration.  
174 The maximum stress reached any point in  $P2$  was determined, and its evolution upon time is summarized in  
175 Figure 6, irrespective of the position on the scallop where it was recorded.

176 Finally, since neochord tensioning was simulated by imposing a displacement, the corresponding force  
177 along the sutures was calculated. Figure 7 describes the variation of the force in time for each of the four  
178 implanted neochords, for both AT (panel a) and 1by1 strategies (panels b-d).

## 179 **DISCUSSION**

180 The MV presents a complex structure that results in a large population variability in both anatomies (e.g.  
181 the number of chordae, leaflets, and annulus shape) and size. Since, the main purpose of the study is to  
182 understand the main effects of the tensioning procedure of artificial chords during the NeoChord  
183 implantation and to generalize the results regardless the patient-specific anatomy, a model based on an  
184 idealized morphology of a population average size [21] was adopted to reproduce the MV apparatus and  
185 prolapse simulation. MV prolapse repair has the function of restoring proper leaflet coaptation. To this aim,  
186 the computed contact area at the systolic peak,  $A_c$ , normalized over the contact area estimated in healthy  
187 conditions, is chosen to provide an indication of the efficacy of the procedure. The same parameter was  
188 previously adopted in similar works [17], [18], in which the dynamics of the MV is simulated through a  
189 more sophisticated patient-specific model. Results reported in Figure 4 suggest that the restoration of MV  
190 functionality is achieved for both AT and 1by1 strategies.

191 For the AT strategy, the achieved coaptation area is about 95 % of the healthy value  $A_{c,H}$ ; whilst with the  
192 1by1 strategy  $A_{c,H}$  is matched or even slightly exceeded. It is also worth noting that, in the case of the 1by1  
193 scheme, the first neochord tensioning already results into a coaptation area equal to the 90 % of  $A_{c,H}$ ,  
194 suggesting that MV restoration could be achieved by means of just one suture, for the present type of  
195 prolapse. However, as discussed below, the use of multiple chords allows to better diffuse stresses over a  
196 larger leaflet region, similarly to the physiological case, and distribute the load between the different  
197 chords.

198 The stress distribution on the valvular apparatus reported in Figure 5 shows that, for the prolapsed  
199 configuration, portion *P2* experiences stress levels similar to the healthy case, while high-stress regions  
200 appear located at the adjacent portions of *P1* and *P3* scallops, close to the position of native chords  
201 rupture, in agreement with the literature [17]. It is worth noting that the correspondence between the  
202 present results and those obtained with a patient-specific based model confirms the reliability of the  
203 adopted simplifications. The stress pattern after the procedure is similar to the healthy case, for both *AT*  
204 and *1by1* tensioning. However, in *1by1* simulations significantly higher stress levels are obtained at  
205 different stages of the procedure. In particular, the first chord pulling causes high stress in one region  
206 around the chord insertion site. This effect is clearly mitigated after the second chord pulling, with high  
207 stress redistributed in two smaller regions; then, tensioning of the third and fourth chord reduces only  
208 slightly the amplitude of high stress regions and transfers the stress concentration in proximity to the  
209 external chords insertion. The results are partially supported by the works of Rim et al. 2014, [17], and  
210 Sturla et al. 2015, [18], which focus on the MV restoration by chords replacement considering  
211 neochordoplasty, i.e. a different surgical technique, carried out through the classical open-chest surgery. In  
212 particular, they tested a virtual repair, at peak systole, of prolapsed MV and its mitigation by implanting  
213 different numbers of chordae. The results, both in terms of stress reduction and distribution, on the  
214 posterior leaflet are consistent with the results of the present analysis. In fact, the same pattern of stress is  
215 observed at the end of the procedure, showing the maximum at the external sutures, although it results in  
216 20% lower [17]. In Figure 6, the analysis of the maximum stress on the valve leaflets,  $\sigma_{\max}$ , indicates that the  
217 *1by1* and *AT* strategies give very similar results, reaching values of about 0.9 MPa at the end of the  
218 procedure. These values are larger than the maximum stress estimated in the healthy condition, which is  
219 about 0.75 MPa. It is worth noting that the sequences of pulling in the *1by1* strategies can affect the stress  
220 condition on the leaflets, showing higher values when the first chord is pulled, with a  $\sigma_{\max}$  of about 1.5 MPa  
221 for *1by1a*, and 1.4 MPa with the other tensioning sequences. The tensioning of the other sutures leads to  
222 progressively lower stress levels, and at the end of the implant, we estimated additional stress of 0.9 MPa  
223 in all cases of analysis, except for the *1by1a* strategy, which achieves  $\sigma_{\max} = 1.0$  MPa (see Figure 6).

224 The assumption of isotropic behaviour, taken as an average of the radial and circumferential stress-strain  
225 curves, although may have some minor effects on the final stress distribution on the leaflets, leads to  
226 negligible differences in terms of chords tensioning forces, which are the principal aspect under  
227 investigation and essentially depend on the transvalvular pressure and on the shape of the leaflets.

228 The stress distribution on the leaflets is related to the tensile force measured in the sutures (Figure 7).  
229 Neochords pulled according to the AT procedure are subjected to a symmetrical force distribution, with a  
230 difference of about 30% between the force acting on the central and lateral insertions (0.18 N and 0.27 N,  
231 respectively, see Figure 7a). 1by1 simulations show that the tensioning order affects the measured force.  
232 Specifically, tensioning a chord reduces the force applied to the chords previously pulled, and the reduction  
233 strongly depends upon the maneuver order and chords position. For instance, in the 1by1a case (Figure 7b)  
234 the force on the neochord pulled first (neochord 2) diminishes as soon as neochord 3 is pulled (F reduction  
235 around 50%) with a further reduction, when neochord 1 is pulled (F reduction around 40%); i.e., the force  
236 on a chord reduces as soon as nearby chords become active. Results also show that no symmetry can be  
237 recognized in the final force distribution with respect to either neochord position or tensioning order.  
238 Moreover, the force is found to vary in the range 0.3-0.35 N for the external chords and in the range 0.1-  
239 0.2N for the central one, showing that the maximum force difference between lateral and central artificial  
240 elements can be as large as 80%. The latter finding suggests that a central neochord can possibly result  
241 approximately unloaded at the end of neochords implantation, as reported by surgical clinical practice.

242 In all cases, the force on one neochord is well below the failure force of the suture, which is about 16 N,  
243 according to the GORE-TEX® SUTURE ePTFE manual. Finally, values of end procedure force applied to each  
244 neochord (see Table 3) also show that the overall force on the group does not significantly vary between  
245 the four simulated strategies of pulling, further reinforcing the idea that differences in force repartition is  
246 due to the pulling sequence. In summary, the AT procedure guarantees an almost symmetric distribution of  
247 the tensioning force on the neochords and the minimum stress level during the implant procedure, but  
248 does not fully restore the healthy contact area. 1by1 strategies allow optimizing the coaptation area,  
249 although the post-procedural leaflet' stress results equal to that in the AT procedure, except for the central

250 to lateral tensioning sequence, which presents a higher stress level and it is proved to be the least  
251 appropriate. Furthermore, the 1by1 strategies may lead to almost inactive chords if care is not given to this  
252 aspect.

### 253 **LIMITATION OF THE STUDY**

254 The present study is limited to the P2 central prolapse, i.e. the most common MV prolapse. A different  
255 stress force distribution may be expected for the lateral (P1-P2 or P2-P3) and the anterior (A) prolapse. In  
256 particular, in the former, due to its asymmetry, the tensioning of the suture is more likely to depend on the  
257 pulling strategy.

258 The use of membrane elements instead of shell elements, neglecting the response to bending, leads to  
259 some minor change in the contact area which, due to the higher flexibility of the selected element, can  
260 result a bit overestimated. Consequently, stresses on the leaflets can result slightly lower (up to 10%),  
261 whereas the force exerted by the sutures does not experience any significant change.

262 The use of both more realistic geometric configuration and more physiologic boundary condition can  
263 further improve the results and highlight additional aspects of the NeoChord implant. It can be foreseen  
264 that, lastly, application of the presented approach to patient-specific anatomies may provide a useful tool  
265 for procedural planning, improving the efficacy of the treatment.

### 266 **CONCLUSIONS**

267 The present investigation compares the two most common tensioning procedures adopted in the  
268 transapical neochords implantation for mitral valve prolapse repair, i.e. 'all together' and 'one by one'  
269 pulling approach. The study was performed on a generalized MV morphology, with prolapsed P2 scallop.

270 Although idealized geometries and simplified constitutive behaviors were assumed, the study captures  
271 some of the clinical effects observed by surgeons, e.g. the unloading of previously pulled neochords.

272 The close similarity between healthy and repaired configuration obtained for all investigated strategies  
273 confirms the reliability and efficacy of the preferred surgical choice of four chords to treat the prolapse  
274 here considered.

275 Differences found in the results concerning coaptation area, stress distribution, and force on the neochords  
276 for AT and 1by1 repair suggest that the 1by1 lateral to central and lateral to lateral approaches are the  
277 most suitable solutions to reach maximum coaptation and maintaining operative leaflets stresses closer to  
278 those experienced in healthy conditions. AT strategy appears more conservative in terms of maximum  
279 stress during the intra-operative insertions since all the chords are activated at the same time, though this  
280 happens at the expense of the optimal valve closure.

281 Though this first study was based on a generalized symmetrical model, the robustness and reduced  
282 computational cost of the presented methodological approach makes it is suitable to be adopted for the  
283 clinical planning of the treatment in patient-specific cases. In addition, this model can represent the first  
284 step towards a more sophisticated platform, using patient-specific images to optimize the surgical  
285 procedure.

## 286 **Acknowledgments**

287 Authors thank Fondazione Cariparo, Padova, Italy, for funding Ph.D. fellowship of Luigi Di Micco. The  
288 Fondazione Cariparo had no involvement in the study design, in the collection, analysis, and interpretation  
289 of data, in the writing of the manuscript, and in the decision to submit the manuscript for publication.

290 This research has been also partially supported by the Fondazione Ing. Aldo Gini, Padova, Italy.

## 291 **Declarations**

292 *Competing interests:* None of the authors has any relationship with industry or financial associations that  
293 might pose a conflict of interest in connection with this work.

294 *Funding:* Fondazione Cariparo, Padova, Italy and Fondazione Ing. Aldo Gini, Padova, Italy.

295 *Ethical approval:* Not required.

296

297 **REFERENCES**

- 298 [1] G. Biglino, C. Capelli, J. Bruse, G. M. Bosi, A. M. Taylor, and S. Schievano, "Computational modelling  
299 for congenital heart disease: How far are we from clinical translation?," *Heart*, vol. 103, no. 2, pp.  
300 98–103, 2017.
- 301 [2] R. Toninato, J. Salmon, F. M. Susin, A. Ducci, and G. Burriesci, "Physiological vortices in the sinuses of  
302 Valsalva: An in vitro approach for bio-prosthetic valves," *J. Biomech.*, vol. 49, no. 13, pp. 2635–2643,  
303 2016.
- 304 [3] G. Burriesci, P. Peruzzo, F. M. Susin, G. Tarantini, and A. Colli, "In vitro hemodynamic testing of  
305 Amplatzer plugs for paravalvular leak occlusion after transcatheter aortic valve implantation," *Int. J.*  
306 *Cardiol.*, vol. 203, pp. 1093–1099, 2016.
- 307 [4] E. Votta *et al.*, "Toward patient-specific simulations of cardiac valves: State-of-the-art and future  
308 directions," *J. Biomech.*, vol. 46, no. 2, pp. 217–228, 2013.
- 309 [5] F. M. Susin, V. Tarzia, T. Bottio, V. Pengo, A. Bagno, and G. Gerosa, "In-vitro detection of thrombotic  
310 formation on bileaflet mechanical heart valves.," *J. Heart Valve Dis.*, vol. 20, no. 4, pp. 378–386,  
311 2011.
- 312 [6] A. Choi, D. D. Mcpherson, and H. Kim, "Computational virtual evaluation of the effect of  
313 annuloplasty ring shape," *Int. j. numer. method. biomed. eng.*, vol. 02831, no. September, pp. 1–11,  
314 2016.
- 315 [7] A. F. Members *et al.*, "Guidelines on the management of valvular heart disease (version 2012) The  
316 Joint Task Force on the Management of Valvular Heart Disease of the European Society of  
317 Cardiology (ESC) and the European Association for Cardio-Thoracic Surgery (EACTS)," *Eur. Heart J.*,  
318 vol. 33, no. 19, pp. 2451–2496, 2012.
- 319 [8] R. A. Nishimura *et al.*, "2014 AHA/ACC guideline for the management of patients with valvular heart  
320 disease," *Circulation*, p. CIR--0000000000000031, 2014.

- 321 [9] J. G. Castillo, J. Solís, Á. González-Pinto, and D. H. Adams, "Surgical Echocardiography of the Mitral  
322 Valve," *Rev. Española Cardiol. (English Ed.)*, vol. 64, no. 12, pp. 1169–1181, 2011.
- 323 [10] A. Colli, E. Bizzotto, D. Pittarello, and G. Gerosa, "Beating heart mitral valve repair with neochordae  
324 implantation: Real-time monitoring of haemodynamic recovery," *Eur. J. Cardio-thoracic Surg.*, vol.  
325 52, no. 5, pp. 991–992, 2017.
- 326 [11] A. Colli, R. Bellu, D. Pittarello, and G. Gerosa, "Transapical off-pump Neochord implantation on  
327 bileaflet prolapse to treat severe mitral regurgitation," *Interact. Cardiovasc. Thorac. Surg.*, p. ivv192,  
328 2015.
- 329 [12] A. Colli *et al.*, "Acute safety and efficacy of the NeoChord procedure," *Interact. Cardiovasc. Thorac.*  
330 *Surg.*, vol. 20, no. 5, pp. 575–581, 2015.
- 331 [13] P. Bajona, K. J. Zehr, J. Liao, and G. Speziali, "Tension Measurement of Artificial Chordae Tendinae  
332 Implanted Between the Anterior Mitral Valve Leaflet and the Left Ventricular Apex An In Vitro  
333 Study," vol. 3, no. 1, pp. 33–37, 2008.
- 334 [14] P. Bajona, W. E. Katz, R. C. Daly, K. J. Zehr, and G. Speziali, "Beating-heart, off-pump mitral valve  
335 repair by implantation of artificial chordae tendineae: An acute in vivo animal study," *J. Thorac.*  
336 *Cardiovasc. Surg.*, vol. 137, no. 1, pp. 188–193, 2009.
- 337 [15] H. Jensen *et al.*, "Transapical neochord implantation: Is tension of artificial chordae tendineae  
338 dependent on the insertion site?," *J. Thorac. Cardiovasc. Surg.*, vol. 148, no. 1, pp. 138–143, 2014.
- 339 [16] M. S. Reimink, K. S. Kunzelman, E. D. Verrier, and R. P. Cochran, "The Effect of Anterior Chordal  
340 Replacement on Mitral Valve Function and Stresses: A Finite Element Study.," *Asaio J.*, vol. 41, no. 3,  
341 pp. M754--M762, 1995.
- 342 [17] Y. Rim, S. T. Laing, D. D. McPherson, and H. Kim, "Mitral Valve Repair Using ePTFE Sutures for  
343 Ruptured Mitral Chordae Tendineae : A Computational Simulation Study," *Ann. Biomed. Eng.*, vol.  
344 42, no. 1, pp. 139–148, 2014.

- 345 [18] F. Sturla *et al.*, “Biomechanical drawbacks of different techniques of mitral neochordal implantation:  
346 When an apparently optimal repair can fail,” *J. Thorac. Cardiovasc. Surg.*, vol. 150, no. 5, pp. 1303–  
347 1312, 2015.
- 348 [19] A. E. Morgan, J. L. Pantoja, E. A. Grossi, L. Ge, J. W. Weinsaft, and M. B. Ratcliffe, “Neochord  
349 placement versus triangular resection in mitral valve repair: A finite element model,” *J. Surg. Res.*,  
350 vol. 206, no. 1, pp. 98–105, 2016.
- 351 [20] G. Gaidulis, E. Votta, M. Selmi, and S. Aidietien, “Numerical simulation of transapical off-pump mitral  
352 valve repair with neochordae implantation,” *Technol. Heal. Care*, vol. 26, 2018.
- 353 [21] K. D. Lau, V. Diaz, P. Scambler, and G. Burriesci, “Medical Engineering & Physics Mitral valve  
354 dynamics in structural and fluid – structure interaction models,” *Med. Eng. Phys.*, vol. 32, no. 9, pp.  
355 1057–1064, 2010.
- 356 [22] K. S. Kunzelman, D. R. Einstein, and R. P. Cochran, “Fluid-structure interaction models of the mitral  
357 valve: Function in normal and pathological states,” *Philos. Trans. R. Soc. B Biol. Sci.*, vol. 362, no.  
358 1484, pp. 1393–1406, 2007.
- 359 [23] A. Avanzini, G. Donzella, and L. Libretti, “Functional and structural effects of percutaneous edge-to-  
360 edge double-orifice repair under cardiac cycle in comparison with suture repair,” *Proc. Inst. Mech.*  
361 *Eng. Part H J. Eng. Med.*, vol. 225, no. 10, pp. 959–971, 2011.
- 362 [24] A. Avanzini, “A Computational Procedure for Prediction of Structural Effects of Edge-to-Edge Repair  
363 on Mitral Valve,” *J. Biomech. Eng.*, vol. 130, no. 3, p. 031015, 2008.
- 364 [25] F. Dal Pan, G. Donzella, C. Fucci, and M. Schreiber, “Structural effects of an innovative surgical  
365 technique to repair heart valve defects,” *J. Biomech.*, vol. 38, no. 12, pp. 2460–2471, 2005.
- 366 [26] B. Prescott, C. J. Abunassar, K. P. Baxevanakis, and L. Zhao, “Computational evaluation of mitral  
367 valve repair with MitraClip,” *Vessel Plus*, vol. 2019, pp. 0–10, 2019.
- 368 [27] K. May-Newman and F. C. Yin, “Biaxial mechanical behavior of excised porcine mitral valve leaflets,”

- 369 *Am. J. Physiol. Circ. Physiol.*, vol. 269, no. 4, pp. H1319--H1327, 1995.
- 370 [28] K. Kunzelman, M. S. Reimink, E. D. Verrier, R. P. Cochran, and R. W. M. Frater, "Replacement of  
371 Mitral Valve Posterior Chordae Tendineae with Expanded Polytetrafluoroethylene Suture: A Finite  
372 Element Study," *J. Card. Surg.*, vol. 11, no. 2, pp. 136–145, 1996.
- 373 [29] A. Colli *et al.*, "Transapical off-pump mitral valve repair with Neochord Implantation (TOP-MINI):  
374 step-by-step guide," *Ann. Cardiothorac. Surg.*, vol. 4, no. 3, p. 295, 2015.
- 375 [30] H. Muresian, "The clinical anatomy of the mitral valve," *Clinical Anatomy*, vol. 22, no. 1. pp. 85–98,  
376 2009.
- 377 [31] Y. Rim *et al.*, "Uncertainty quantification of inflow boundary condition and proximal arterial stiffness  
378 coupled effect on pulse wave propagation in a vascular network," *Ann. Biomed. Eng.*, vol. 9, no. 1,  
379 pp. 85–98, 2016.
- 380 [32] E. Votta, E. Caiani, F. Veronesi, M. Soncini, F. M. Montevicchi, and A. Redaelli, "Mitral valve finite-  
381 element modelling from ultrasound data: a pilot study for a new approach to understand mitral  
382 function and clinical scenarios," *Philos. Trans. R. Soc. A Math. Phys. Eng. Sci.*, vol. 366, no. 1879, pp.  
383 3411–3434, 2008.
- 384 [33] A. Colli *et al.*, "Prognostic impact of leaflet-to-annulus index in patients treated with transapical off-  
385 pump echo-guided mitral valve repair with NeoChord implantation," *Int. J. Cardiol.*, vol. 257, no.  
386 November 2015, pp. 235–237, 2018.
- 387 [34] A. Colli *et al.*, "Transapical off-pump mitral valve repair with Neochord implantation: Early clinical  
388 results," *Int. J. Cardiol.*, vol. 204, pp. 23–28, 2016.
- 389 [35] A. Colli *et al.*, "CT for the Transapical Off-Pump Mitral Valve Repair With Neochord Implantation  
390 Procedure," *JACC Cardiovasc. Imaging*, vol. 10, no. 11, pp. 1397–1400, 2017.

391

392 **FIGURES AND TABLES**

393 **Table 1.** Dimensional parameters adopted for leaflets and chordae of the MV model. Data were set in  
 394 accordance with [18] and [17]. APD and CD indicate the ateropostirial and commissures distance,  
 395 respectively.

<b>Leaflets</b>				
	<b>Anterior</b>	<b>Posterior</b>		<b>Commissure</b>
		<b>P2</b>	<b>P1/P3</b>	
<b>Height (mm)</b>	20	13.8	11.2	8.8
<b>Ann. Lenght (mm)</b>	32.3	17.5	12.7	6.7
<b>Area (mm<sup>2</sup>)</b>	457.6	204.4	123.9	51.2
<b>Thickness (mm)</b>	0.69	0.51		0.6
<b>Chordae Tendineae</b>				
<b>Cross-sectional area (mm<sup>2</sup>)</b>	0.29	0.27		0.28
<b>Annulus</b>				
<b>APD (mm)</b>	22			
<b>CD (mm)</b>	30			
<b>Area (mm<sup>2</sup>)</b>	552.7			

396

397 **Table 2.** Determined coefficients of equation (1) for anterior and posterior leaflets. (All units in MPa)

398

	<b>D<sub>1</sub></b>	<b>C<sub>10</sub></b>	<b>C<sub>20</sub></b>	<b>C<sub>30</sub></b>	<b>C<sub>40</sub></b>	<b>C<sub>50</sub></b>
<b>Anterior leaflet</b>	4.999	0.008	-0.073	0.742	-3.093	4.635
<b>Posterior leaflet</b>	6.564	0.006	0.001	0.015	-0.045	0.037

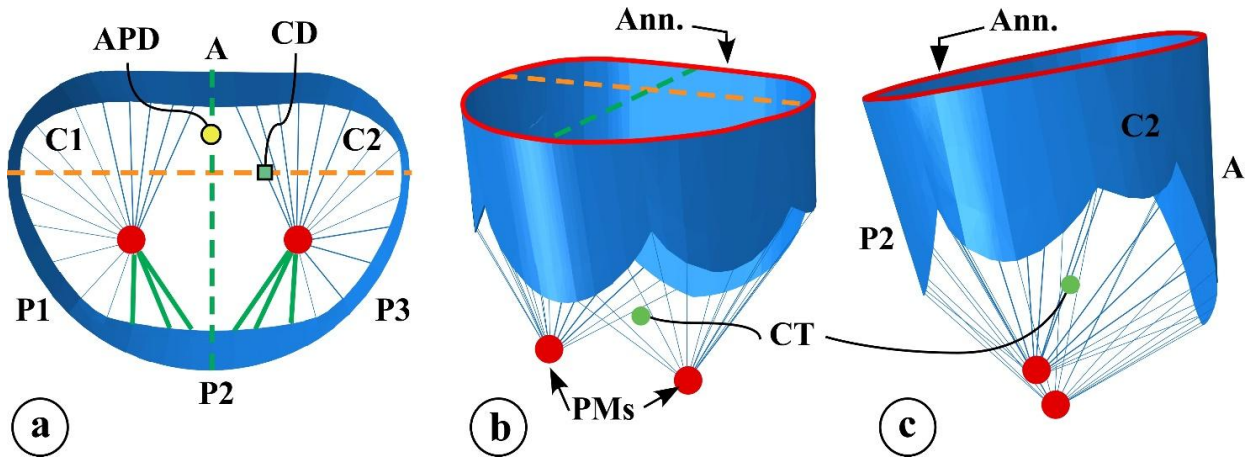
399

400 **Table 3.** Forces calculated on the neochords after the implantation of the four cases analyzed. Forces are  
 401 expressed in *N*

	<b>neochord</b>				<b>Tot</b>
	<b>a</b>	<b>b</b>	<b>c</b>	<b>d</b>	
<b>AT</b>	0.27	0.17	0.18	0.27	0.89
<b>Iby1a</b>	0.34	0.10	0.20	0.28	0.92
<b>Iby1b</b>	0.32	0.11	0.19	0.28	0.90
<b>Iby1c</b>	0.32	0.11	0.19	0.29	0.91

402

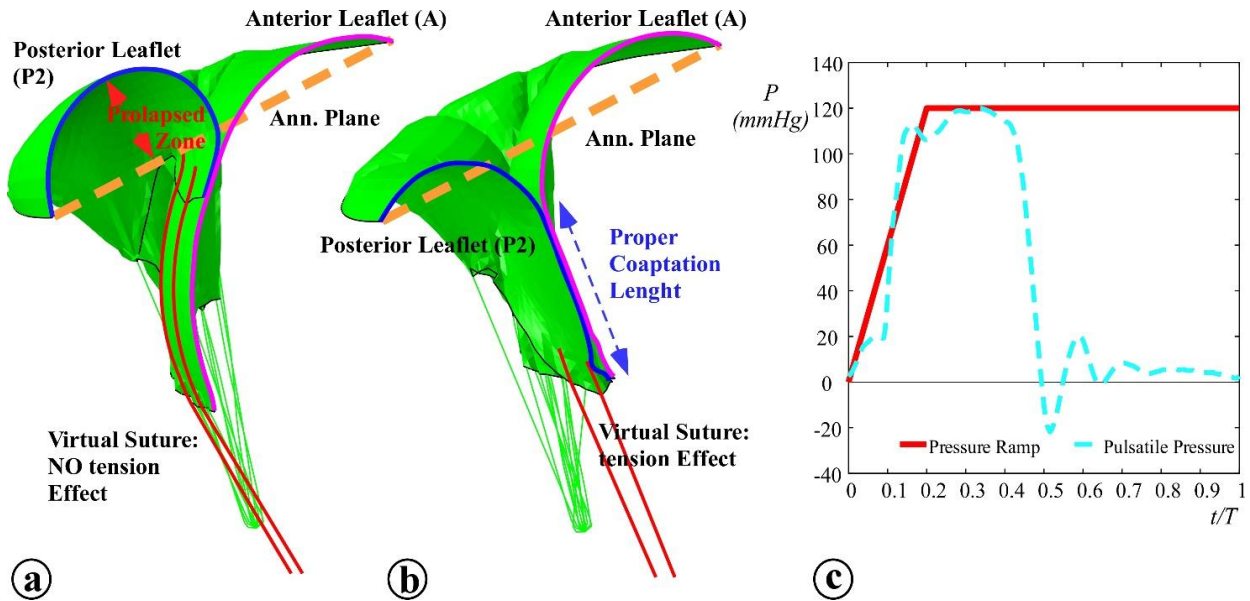
403



404

405 **Figure 1.** MV geometry of the model at the end of diastole. **a)** Atrial to ventricle view: A indicates the  
 406 anterior leaflet, C1 and C2 the commissural leaflet scallops, P1, P2 and P3 the posterior leaflet scallops, and  
 407 APD and CD the ateropostirial and commissures distance, respectively. **b)** Perspective view: red lines  
 408 indicates MV annulus. CT the chordae thendinae, and PMs the papillary muscles. **c)** Lateral view. The  
 409 chordae thendinae in green have been cut off to generate prolapse.

410

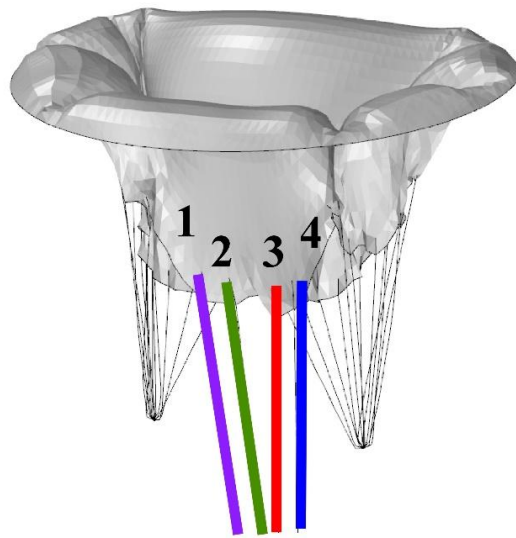


411

412 **Figure 2.** Restoration of MV. **a)** P2 prolapse before the tensioning of neochords (red lines). **b)** P2 prolapse  
 413 mitigation due to the tensioning of the neochords. Virtual sutures are inserted 3 mm far from leaflet free  
 414 margin. The contact line between anterior (magenta line) and posterior (blue line) leaflet determines the  
 415 coaptation length. **c)** Comparison between pulsatile (dotted line) and steady pressure condition (solid line)  
 416 linearly reached. The latter was applied to the ventricular surface of the valve for all simulation.

417

418

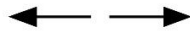


**All together strategy (AT)**

$$1 = 2 = 3 = 4$$

**One by one strategies (1by1)**

*a) Central to Lateral: 2;3;4;1*



*b) Lateral to Central: 1;4;2;3*



*c) Lateral to Lateral: 1;2;3;4*

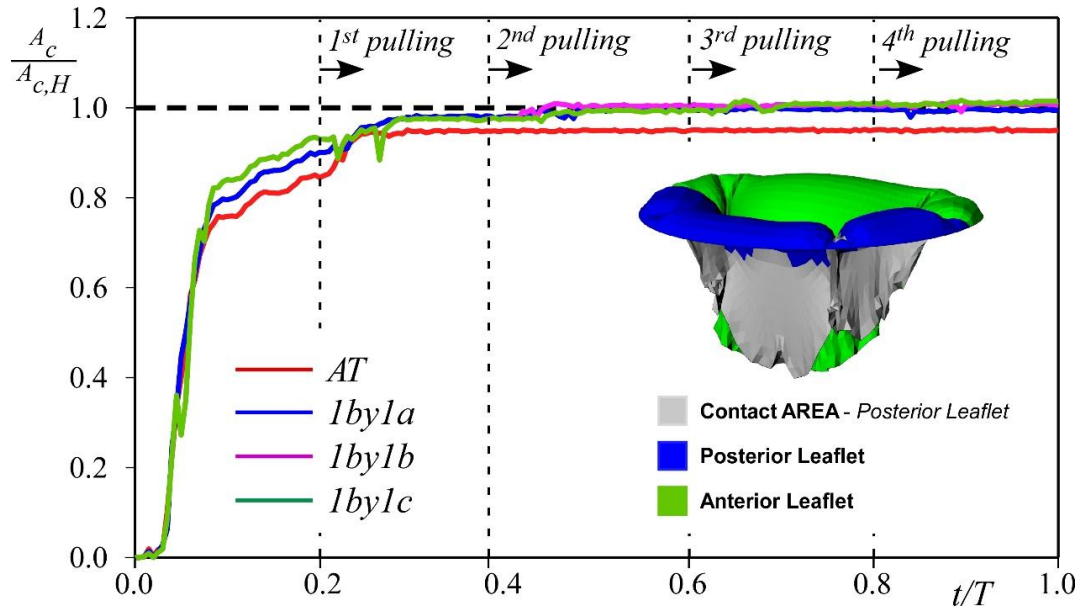


419

420 **Figure 3.** Simulated protocol tensiometer. In AT procedure all neochords are pulled together. In 1by1  
 421 procedure the chords are pulled one by one following three sequences: *a) central to lateral*, *b) lateral to*  
 422 *central*, and *c) lateral to lateral*. In all simulations, neochords are numbered in crescent order starting from  
 423 left external position to right external position.

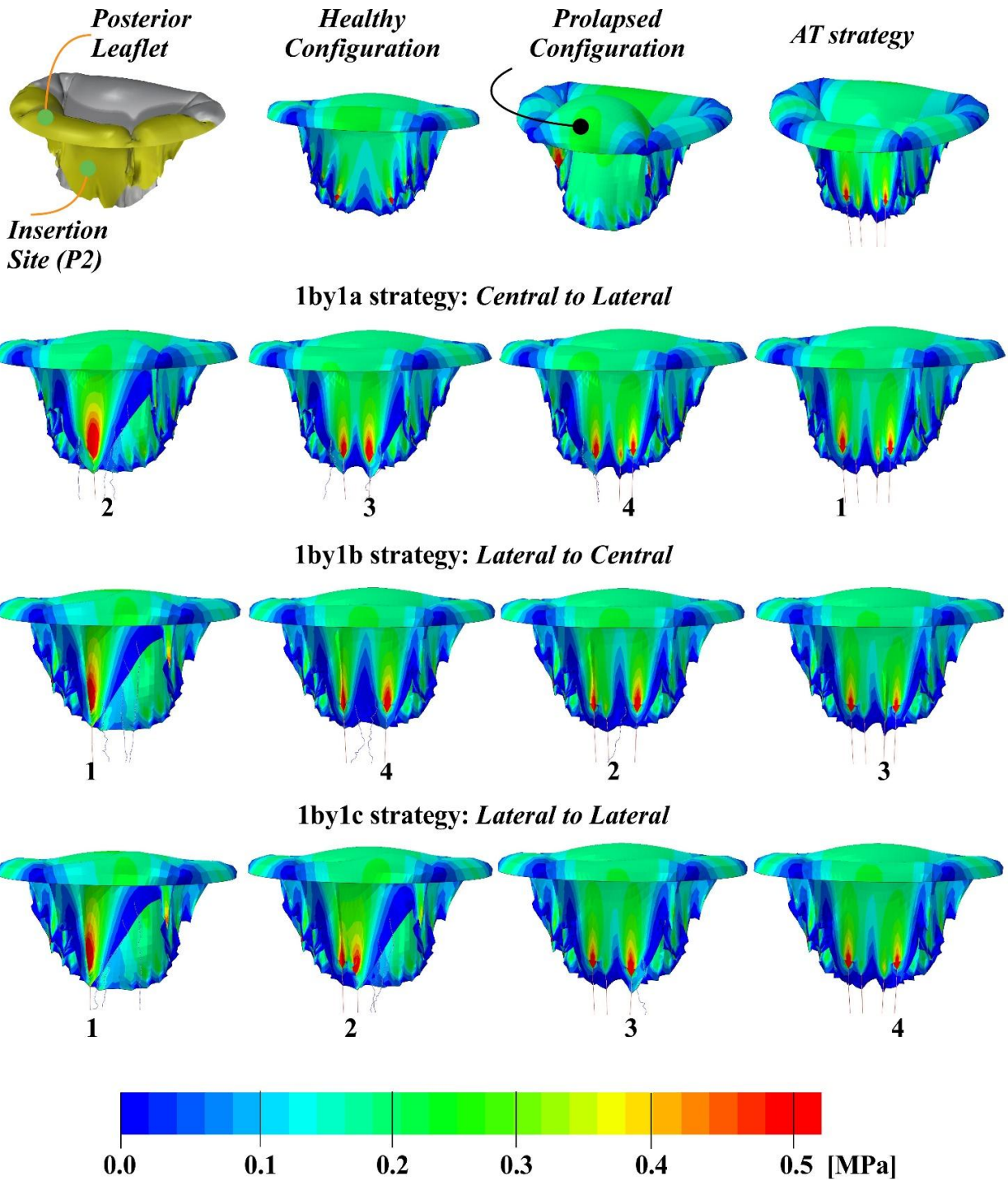
424

425



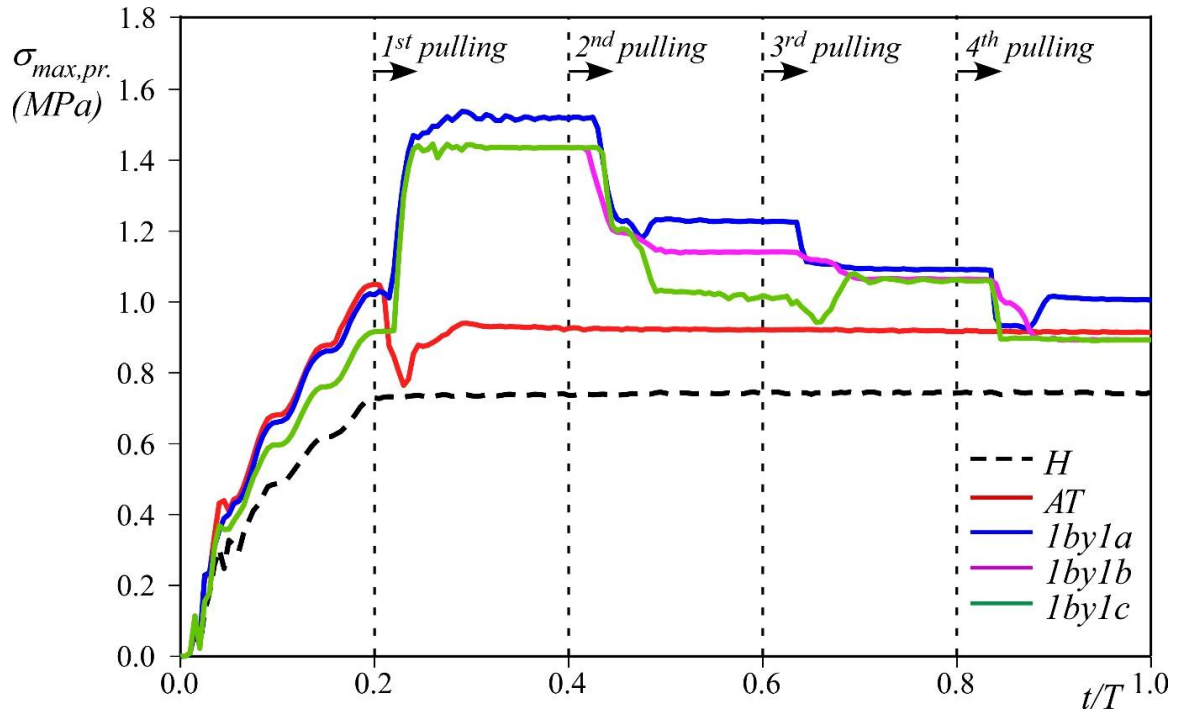
426

427 **Figure 4.** Overall contact area on the Posterior leaflet during chord tensioning normalized with the contact  
 428 area of the healthy configuration  $A_{c,H}$ . Red line represents *AT strategy*, blue, magenta and green lines  
 429 represent *lby1 strategies* following sequence *a)*, *b)* and *c)* of Figure 3, respectively.



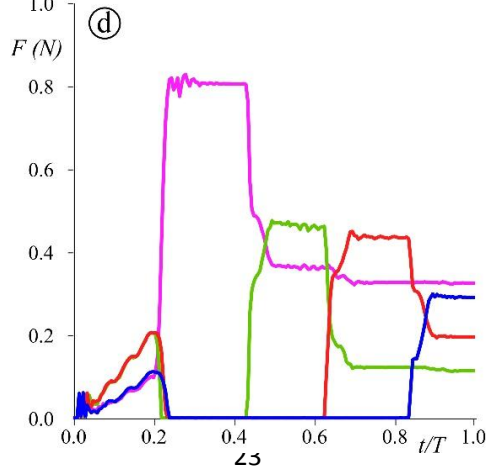
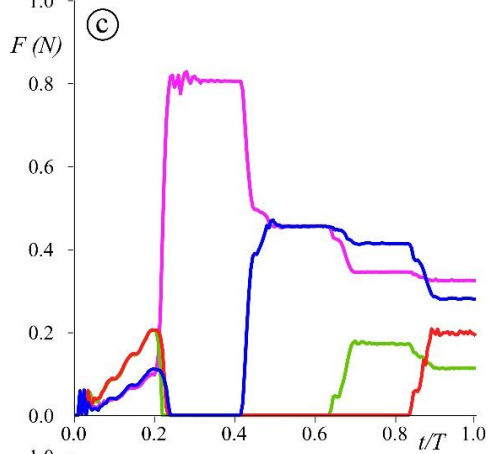
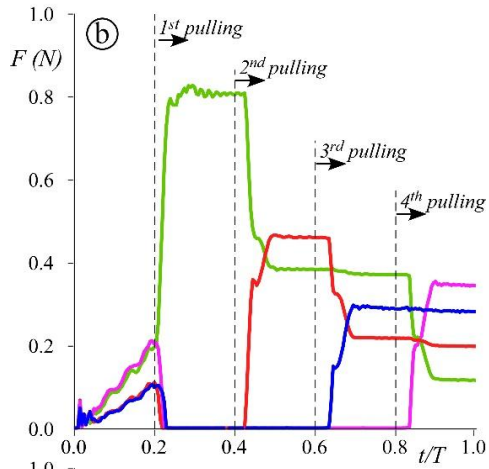
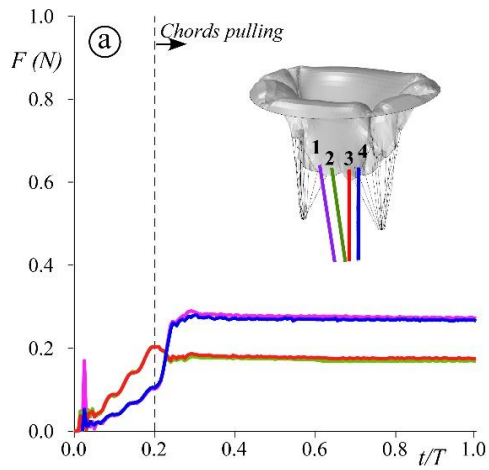
431

432 **Figure 5.** MV stress patterns at systolic peak. Leaflet stress in *healthy configuration*, *prolapsed configuration*  
 433 with inactive neochords, *AT strategy* configuration, and *1by1 strategy* at different steps of pulling. The  
 434 stress field in 1by1 cases is reported after the complete load of the neochord labeled by the irrespective  
 435 number.



437

438 **Figure 6.** Maximum principal stress calculated on the P2 scallop during simulations. The black dotted line  
 439 represents the stress calculated for the Healthy configuration (*H*). The red line represents the *AT* strategy.  
 440 The blue, magenta and green lines represent *1by1* strategies following sequence *a*), *b*) and *c*) of Figure 3,  
 441 respectively.



443 **Figure 7.** Force applied by neochords during the implant in **a)** *AT strategy*, **b)** *1by1a (central to lateral*  
444 *sequence)*, **c)** *1by1b (lateral to central sequence)*, and **d)** *1by1c (lateral to lateral sequence)*.

1 **Original Article**

2 **The Neochord Mitral Valve Repair Procedure: Numerical Simulation of Different Neochords Tensioning**

3 **Protocols**

4 *Luigi Di Micco<sup>1</sup>, Paolo Peruzzo<sup>1</sup>, Andrea Colli<sup>2</sup>, Gaetano Burriesci<sup>3,4</sup>, Daniela Boso<sup>1</sup>, Laura Besola<sup>2</sup>, Gino*

5 *Gerosa<sup>2</sup> & Francesca M. Susin<sup>1</sup>*

6 1 Cardiovascular Fluid Dynamics Laboratory, ICEA Department, University of Padova, Italy;

7 2 DSCTV, University of Padova Medical School, Italy;

8 3 UCL Mechanical Engineering, University College London, United Kingdom;

9 4 Ri.MED Foundation, Palermo, Italy.

10

11 **Corresponding Author:**

12 Luigi Di Micco

13 Cardiovascular Fluid Dynamics Laboratory, ICEA Department

14 University of Padova, Italy

15 Via Loredan 20, 35131 Padova (Italy)

16 phone: +39 049 827 5433

17 e-mail: [luigi.dimicco@dicea.unipd.it](mailto:luigi.dimicco@dicea.unipd.it)

18 **Word count:** 3421

19

20 **Keywords:** NeoChord procedure, Mitral Valve Repair, Finite Elements Analysis, Tensioning Strategies, Mitral

21 Valve Prolapse,

22

23 **ABSTRACT**

24 Transapical off-pump mitral valve repair with neochord implantation is an established technique for  
25 minimally-invasive intervention on mitral valve prolapse/flail. The procedure involves the positioning of  
26 artificial chords, whose length/tension is adjusted intraoperatively, adopting different methods based on  
27 the experience of the surgeon. This unsystematic approach occasionally leads to complications such as  
28 leaflet rupture and excessive/insufficient load on the neochords. In this study, finite element models of a  
29 generalized prolapsing mitral valve are used to verify the effect of two alternative tensioning approaches  
30 (AT – All together and 1by1 – one by one sequences) on the coaptation area and valve biomechanics,  
31 comparing results with a corresponding healthy configuration. The total force of about 1 N is exerted by the  
32 chords in both strategies, but the maximum stress and coaptation area are closer to those of the healthy  
33 configuration in the 1by1 sequence. However, the analysis also provides an explanation for the chords  
34 unloading in the 1by1 strategy observed in the clinical practice, and suggests an optimum tensioning  
35 methodology for NeoChord procedures. The study also reveals the potential power of the implemented  
36 numerical approach to serve as a tool for procedural planning, supporting the identification of the most  
37 suitable ventricular access site and the most effective stitching points for the artificial chords.

38 **INTRODUCTION**

39 Experimental and numerical investigations are nowadays largely used to assess the safety and efficacy of  
40 cardiovascular devices and procedures, by identifying an enhanced medical practice and support clinical  
41 decisions [1]–[6]. However, the application of these approaches to treatments of mitral valve (MV) diseases  
42 still represents a major challenge, due to the complex anatomy of the valvular and subvalvular apparatus.

43 Mitral regurgitation (MR) is one of the most complex valvular diseases. MR is classified into two categories:  
44 functional MR (FMR), due to left ventricular (LV) dilation and dysfunction, and degenerative MR (DMR), due  
45 to a structural abnormality of the valve apparatus, mainly. The latter can lead, among possible valve  
46 failures, to prolapse or flail [7]–[9]. Recently a new MV procedure with off-pump transcatheter access with  
47 neochord implantation has emerged as a new promising surgical procedure to restore the functionality of  
48 DMR [10], [11]. It consists in the replacement of native chordae tendineae with artificial tethers, inserted

49 by transapical access. The clinical outcome has confirmed the safety and effectiveness of the approach [12],  
50 enlightening the issues to be addressed to enhance the reliability of the procedure and support  
51 preoperative planning. In particular, the optimum tensioning of the artificial chords still needs to be  
52 determined, in order to maximize the efficacy of the technique and the durability of the solution [13]. This  
53 issue is further complicated by the fact that the transapical implantation approach results in non-  
54 physiological orientations of the artificial sutures, which load the leaflet along directions different from the  
55 native chordae

56 A number of in vitro and in silico studies have attempted to study the biomechanics of MV repair with neo-  
57 chords implantation [14]–[19] analysing the post-implant configuration after the complete surgical  
58 procedure. Differently by the cited studies, the NeoChord procedure is performed in beating-heart.  
59 Consequently, in order to identify the most suitable implantation protocol and the commonly reported  
60 procedural complications, such as leaflet rupture or neochords overloading/unloading, the study of  
61 NeoChord procedure also requires the investigation of the leaflet coaptation and stress pattern during the  
62 chords positioning, i.e. during the operative phase of the implant procedure. Recently, a FEM analysis was  
63 developed in order to evaluate the sutures length effect in MV repair with transapical neochord  
64 implantation [20]. ~~However, The latter is~~ the main focus of ourthe present study ~~and it~~ consists in analysing  
65 the procedural and post-implant outcome of the two strategies currently in use for neochords tensioning  
66 during the repair:

- 67 • the *'all together'* strategy, i.e. all chords are tensioned contemporarily all together;
- 68 • the *'one by one'*, i.e. the chords are tensioned one at the time by subsequently applying to each  
69 chord a proper tensioning with a certain order.

70 For both tensioning strategies, the intraoperative behavior of leaflet coaptation, the stress distribution in  
71 the valve apparatus, and the tensioning force in each chord are determined by means of numerical  
72 simulations of a generalised MV prolapse.

## 73 METHODS

### 74 Mitral valve model

75 Healthy MV prevents blood backflow from the left ventricle to atrium during systole by coaptation of  
76 posterior and anterior leaflets; a number of tendinous strings (*chordae tendinae*) contribute to holding the  
77 closed valve in place, by tethering the leaflets to the ventricular wall via papillary muscles structure. ~~Such a  
78 complex structure also results in a large population variability in both anatomies (e.g. the number of  
79 chordae, leaflets, and annulus shape) and size. Since, the main purpose of the study is to understand the  
80 main effects of the tensioning procedure of artificial chords during the NeoChord implantation and to  
81 generalize the results regardless the patient specific anatomy, a model based on an idealized morphology  
82 of a population average size [20] was adopted to reproduce the MV apparatus (see Figure 1).~~

83 Leaflets were designed to include the common anatomical segments usually identified, including the  
84 anterior leaflet scallop, *A*; the commissural leaflet scallops, *C1* and *C2*; the posterior leaflet scallops *P1*, *P2*,  
85 and *P3*, as represented in Figure 1. All main parameters of valve geometry, e.g. the thickness and cross-  
86 sectional area used for the leaflets and chordae in the various portions of the model, are summarized in  
87 Table 1.

88 Since the proposed study is concerned essentially with the systolic phase, the dynamic motion of the  
89 annulus and papillary muscles were not simulated, keeping the annular profile fixed on a plane and  
90 maintaining a constant distance between the annulus plane and the papillary muscles (idealized as  
91 anchoring points - red dots in Figure 1). These assumptions, which are common in the literature [21], [22],  
92 are considered acceptable due to the comparative nature of this study.

93 Leaflets were modeled as membranes, with the isotropic hyperelastic incompressible constitutive law  
94 based on a 5<sup>th</sup> order reduced polynomial strain energy potential formulation. ~~A~~ [According to previous works  
95 concerning the analysis of MV repair \[23\]–\[26\], \*U\* that](#) reads:

$$U = \sum_{i=1}^5 C_{i0} (\bar{I}_1 - 3)^i + \sum_{i=1}^5 \frac{1}{D_i} (J_{el} - 1)^{2i} \quad (1)$$

96

97 Where  $\bar{I}_1$  is the first deviatoric strain invariant  $\bar{I}_1 = \bar{\lambda}_1^2 + \bar{\lambda}_2^2 + \bar{\lambda}_3^2$ , where  $\bar{\lambda}_i = J^{-\frac{1}{3}}\lambda_i$  are the deviatoric  
98 stretches, with  $J$  the total volume ratio and  $\lambda_i$  the principal stretches;  ~~$J_{et}$  is the elastic volume strain,~~  
99 ~~defined as  $J_{et} = \frac{J}{J^{th}}$ , being  $J^{th}$  the thermal volume ratio as function of the linear thermal expansion  $\epsilon^{th}$ ,~~  
100 ~~according to  $J^{th} = (1 + \epsilon^{th})^3$ .~~  $C_{i0}$  and  $D_i$  are the coefficients determined from mechanical tests  
101 performed on porcine mitral valves [27], averaging data obtained along radial and circumferential direction,  
102 and they are summarized in table 2. The anisotropy shown by the biaxial tensile tests performed by May-  
103 Newman appears rather reduced and, given the comparative purpose of the present work, it was decided  
104 to assume an isotropic hyperelastic behavior for the leaflet's tissue.

105 Chords were modelled as linear elastic trusses, with Young modulus ( $E$ ) equal to 40 MPa (Kunzelman et al.,  
106 1996; Lau et al., 2010);

107 In the neochord procedure, artificial chords are usually obtained from e-PTFE *CV-4 Gore-Tex* sutures with a  
108 cross-section of 0.074 mm<sup>2</sup>, tied to the leaflet margin with a girth hitch knot approach, resulting in two  
109 suture stands pulled in the same direction [29]. In the model, each artificial chord was represented by  
110 linear truss element with a circular cross-section of 0.148 mm<sup>2</sup> (i.e. equal to the sum of the cross-section of  
111 the two stands). The neochord's Young modulus was determined experimentally by performing tension  
112 testing on an e-PTFE wire. For the test, the wire was settled on the tensile testing machine (Zwick-Roll,  
113 *Zwick GmbH & Co.KG, Zwick USA*) in a wet environment of saline solution at a temperature of 37°, to  
114 recreate physiological conditions. A 40 mm initial length was used, i.e. the length of the neochords in the  
115 numerical model. Results suggested a value of the Young modulus equal to 2.3 GPa for the *CV-4 Gore-Tex*  
116 *suture*.

## 117 **Simulations**

118 The mitral valve was modeled by using the explicit approach with the finite element code ABAQUS  
119 (SIMULIA, Providence, RI). Leaflets and chords were represented by linear triangular membrane elements  
120 (2D elements) and truss (1D elements), respectively. The connections between the leaflets free-margin and  
121 the chordae tendineae were modeled simulating the physiological intra-leaflets insertion of the native

122 chords as described by Muresian (2009) ,[31], on the basis of an accurate clinical analysis. In the model,  
123 along with the free-margin insertion, the native chordae elements were prolonged inside the leaflets by  
124 sharing the same nodes discretization for three nodes, thus avoiding unrealistic stress concentration and  
125 singularity points.

126 The nodes describing the annulus were fixed in space, allowing rotations of the leaflets elements about all  
127 axes. Similarly, the chordae were pinned at the nodes corresponding to the papillary muscles. The unloaded  
128 valve model was generated in a fully open position [32].

129 The closed configuration was achieved by applying a spatially uniform pressure on the ventricular side.  
130 Since the model does not describe the annulus and papillary muscles dynamics occurring during the cardiac  
131 cycle, some preliminary simulations were performed to verify the effect of the load history on the systolic  
132 configuration. In particular, the comparison between the values of the maximum principal stresses at the  
133 peak load, which were obtained applying physiologically pulsatile pressures and steady pressure conditions  
134 reached by ramping the load linearly (Figure 2c), indicated lower stress in pulsatile condition, with  
135 differences inferior to 10%. Differences in term of displacement were negligible and inferior to 0.5%.  
136 Hence, the decision was taken to apply a spatially uniform pressure linearly increasing from 0 to 120 mmHg  
137 in 200 ms (corresponding to the systolic peak) to the ventricular side of the valve, for all analyzed cases.  
138 This approach significantly reduced the overall computational cost of the simulations, as well.

139 A reference model, including the presence and healthy function of all chordae, was run to estimate the  
140 optimal anterior-posterior leaflets coaptation achievable with the selected MV description (see Figure 1). A  
141 MV incompetence was then simulated by detaching six central chords (see green chords in Figure 1),  
142 leading to a central width prolapse (P2 section in Figure 2a) that is the most common leaflet disease for  
143 patients who underwent NeoChord repair [33].

144 In the prolapsed scenario, the repair was simulated by adding four artificial neochords between the margin  
145 of the prolapsed leaflets portion and the ventricle entry site (see Figure 2b), [34]. The entry site was located  
146 40 mm apart from the annulus, according to in-vivo measurements, to form the optimal neochord  
147 trajectory implantation [35].

148 In the first stage of the analysis, the four sutures were not tensioned until the maximum pressure load was  
149 achieved (case of implanted but inactive artificial chords to mimic the prolapsed pre-tensioning  
150 configuration) so that the valve reached the idealized prolapse condition before the tensioning. From the  
151 end-diastole configuration, with a linear pressure load from 0 to 120 mmHg, the valve is forced to close.  
152 During this first stage of the simulation, all the artificial sutures implanted were not tensioned (i.e. one side  
153 is attached to the leaflet while the other side was free to move in order to simulate the clinical phase  
154 during which the external sutures remain outside the ventricle before the tensioning stage). In the second  
155 stage of the analysis, two different strategies for restoring the valve coaptation were pursued. In the first  
156 one, indicated as *all together* strategy (AT) the four chords were tensioned contemporarily, by applying the  
157 displacement required to restore leaflets coaptation (Figure 3a). In the second strategy, indicated as *one by*  
158 *one* strategy (1by1), the four chords were tensioned one at the time by subsequently applying to each  
159 chord the same displacement as the AT case. In all simulations, for all the schemes analyzed, the tensioning  
160 was performed by imposing at the proximal nodes of the artificial sutures the same outward displacement  
161 along the longitudinal direction. Such displacement promotes the reduction of the prolapsed portion of the  
162 posterior leaflet, since its margin moves towards the anterior one, until the repaired configuration is  
163 achieved. The prescribed displacement was set equal to 11 mm, to obtain the proper coaptation length.  
164 This value was defined after some preliminary analysis by tuning the chords displacement until the  
165 maximum coaptation length between the anterior and posterior free margin was measured at the anterior-  
166 posterior axis (see Figure 1). In order to compare the two pulling strategies, we chose to prescribe the same  
167 displacement of the sutures in all simulations, coherently with the clinical practice, where clinicians can  
168 easily control the chordae displacement. In order to examine the different strategies commonly adopted by  
169 surgeons when repairing MV prolapse by NeoChord procedure, the following possible sequences of chord  
170 pulling were simulated (figure 3b):

- 171 a) central to lateral pulling (1by1a);
- 172 b) lateral to central (1by1b);
- 173 c) lateral to lateral (1by1c).

174 **RESULTS**

175 The healthy configuration of the generalized MV model produced a leaflets coaptation length along the axis  
176 of symmetry of about 8 mm, corresponding to a total contact area,  $A_{c,H}$ , between the anterior and posterior  
177 leaflet of about 270 mm<sup>2</sup>. The contact area,  $A_c$ , restored during neochords tensioning procedures,  
178 normalized with  $A_{c,H}$  is reported in Figure 4.

179 Figure 5 shows the contour map of the stress field computed on the treated leaflet  $P2$  for all analyzed  
180 configurations. A scale from 0 to 0.5 MPa was chosen to better visualize the areas of stress concentration.  
181 The maximum stress reached any point in  $P2$  was determined, and its evolution upon time is summarized in  
182 Figure 6, irrespective of the position on the scallop where it was recorded.

183 Finally, since neochord tensioning was simulated by imposing a displacement, the corresponding force  
184 along the sutures was calculated. Figure 7 describes the variation of the force in time for each of the four  
185 implanted neochords, for both AT (panel a) and 1by1 strategies (panels b-d).

186 **DISCUSSION**

187 The MV presents such a complex structure that also results in a large population variability in both  
188 anatomies (e.g. the number of chordae, leaflets, and annulus shape) and size. Since, the main purpose of  
189 the study is to understand the main effects of the tensioning procedure of artificial chords during the  
190 NeoChord implantation and to generalize the results regardless the patient-specific anatomy, a model  
191 based on an idealized morphology of a population average size [21] was adopted to reproduce the MV  
192 apparatus and prolapse simulation (see Figure 1).

193 MV prolapse repair has the function of restoring proper leaflet coaptation. To this aim, the computed  
194 contact area at the systolic peak,  $A_c$ , normalized over the contact area estimated in healthy conditions, is  
195 chosen to provide an indication of the efficacy of the procedure. The same parameter was previously  
196 adopted in similar works [17], [18], in which the dynamics of the MV is simulated through a more  
197 sophisticated patient-specific model. Results reported in Figure 4 suggest that the restoration of MV  
198 functionality is achieved for both AT and 1by1 strategies.

199 For the AT strategy, the achieved coaptation area is about 95 % of the healthy value  $A_{c,H}$ ; whilst with the  
200 1by1 strategy  $A_{c,H}$  is matched or even slightly exceeded. It is also worth noting that, in the case of the 1by1  
201 scheme, the first neochord tensioning already results into a coaptation area equal to the 90 % of  $A_{c,H}$ ,  
202 suggesting that MV restoration could be achieved by means of just one suture, for the present type of  
203 prolapse. However, as discussed below, the use of multiple chords allows to better diffuse stresses over a  
204 larger leaflet region, similarly to the physiological case, and distribute the load between the different  
205 chords.

206 The stress distribution on the valvular apparatus reported in Figure 5 shows that, for the prolapsed  
207 configuration, portion  $P2$  experiences stress levels similar to the healthy case, while high-stress regions  
208 appear located at the adjacent portions of  $P1$  and  $P3$  scallops, close to the position of native chords  
209 rupture, in agreement with the literature [17]. It is worth noting that the correspondence between the  
210 present results and those obtained with a patient-specific based model confirms the reliability of the  
211 adopted simplifications. The stress pattern after the procedure is similar to the healthy case, for both  $AT$   
212 and 1by1 tensioning. However, in 1by1 simulations significantly higher stress levels are obtained at  
213 different stages of the procedure. In particular, the first chord pulling causes high stress in one region  
214 around the chord insertion site. This effect is clearly mitigated after the second chord pulling, with high  
215 stress redistributed in two smaller regions; then, tensioning of the third and fourth chord reduces only  
216 slightly the amplitude of high stress regions and transfers the stress concentration in proximity to the  
217 external chords insertion. The results are partially supported by the works of Rim et al. 2014, [17], and  
218 Sturla et al. 2015, [18], which focus on the MV restoration by chords replacement considering  
219 neochordoplasty, i.e. a different surgical technique, carried out through the classical open-chest surgery. In  
220 particular, they tested a virtual repair, at peak systole, of prolapsed MV and its mitigation by implanting  
221 different numbers of chordae. The results, both in terms of stress reduction and distribution, on the  
222 posterior leaflet are consistent with the results of the present analysis. In fact, the same pattern of stress is  
223 observed at the end of the procedure, showing the maximum at the external sutures, although it results in  
224 20% lower [17]. In Figure 6, the analysis of the maximum stress on the valve leaflets,  $\sigma_{max}$ , indicates that the

225 1by1 and AT strategies give very similar results, reaching values of about 0.9 MPa at the end of the  
226 procedure. These values are larger than the maximum stress estimated in the healthy condition, which is  
227 about 0.75 MPa. It is worth noting that the sequences of pulling in the 1by1 strategies can affect the stress  
228 condition on the leaflets, showing higher values when the first chord is pulled, with a  $\sigma_{\max}$  of about 1.5 MPa  
229 for 1by1a, and 1.4 MPa with the other tensioning sequences. The tensioning of the other sutures leads to  
230 progressively lower stress levels, and at the end of the implant, we estimated additional stress of 0.9 MPa  
231 in all cases of analysis, except for the 1by1a strategy, which achieves  $\sigma_{\max} = 1.0$  MPa (see Figure 6).

232 The assumption of isotropic behaviour, taken as an average of the radial and circumferential stress-strain  
233 curves, although may have some minor effects on the final stress distribution on the leaflets, leads to  
234 negligible differences in terms of chords tensioning forces, which are the principal aspect under  
235 investigation and essentially depend on the transvalvular pressure and on the shape of the leaflets.

236 The stress distribution on the leaflets is related to the tensile force measured in the sutures (Figure 7).  
237 Neochords pulled according to the AT procedure are subjected to a symmetrical force distribution, with a  
238 difference of about 30% between the force acting on the central and lateral insertions (0.18 N and 0.27 N,  
239 respectively, see Figure 7a). 1by1 simulations show that the tensioning order affects the measured force.  
240 Specifically, tensioning a chord reduces the force applied to the chords previously pulled, and the reduction  
241 strongly depends upon the maneuver order and chords position. For instance, in the 1by1a case (Figure 7b)  
242 the force on the neochord pulled first (neochord 2) diminishes as soon as neochord 3 is pulled (F reduction  
243 around 50%) with a further reduction, when neochord 1 is pulled (F reduction around 40%); i.e., the force  
244 on a chord reduces as soon as nearby chords become active. Results also show that no symmetry can be  
245 recognized in the final force distribution with respect to either neochord position or tensioning order.

246 Moreover, the force is found to vary in the range 0.3-0.35 N for the external chords and in the range 0.1-  
247 0.2N for the central one, showing that the maximum force difference between lateral and central artificial  
248 elements can be as large as 80%. The latter finding suggests that a central neochord can possibly result  
249 approximately unloaded at the end of neochords implantation, as reported by surgical clinical practice.

250 In all cases, the force on one neochord is well below the failure force of the suture, which is about 16 N,  
251 according to the GORE-TEX® SUTURE ePTFE manual. Finally, values of end procedure force applied to each  
252 neochord (see Table 3) also show that the overall force on the group does not significantly vary between  
253 the four simulated strategies of pulling, further reinforcing the idea that differences in force repartition is  
254 due to the pulling sequence. In summary, the AT procedure guarantees an almost symmetric distribution of  
255 the tensioning force on the neochords and the minimum stress level during the implant procedure, but  
256 does not fully restore the healthy contact area. 1by1 strategies allow optimizing the coaptation area,  
257 although the post-procedural leaflet' stress results equal to that in the AT procedure, except for the central  
258 to lateral tensioning sequence, which presents a higher stress level and it is proved to be the least  
259 appropriate. Furthermore, the 1by1 strategies may lead to almost inactive chords if care is not given to this  
260 aspect.

#### 261 **LIMITATION OF THE STUDY**

262 The present study is limited to the P2 central prolapse, i.e. the most common MV prolapse. A different  
263 stress force distribution may be expected for the lateral (P1-P2 or P2-P3) and the anterior (A) prolapse. In  
264 particular, in the former, due to its asymmetry, the tensioning of the suture is more likely to depend on the  
265 pulling strategy.

266 The use of membrane elements instead of shell elements, neglecting the response to bending, leads to  
267 some minor change in the contact area which, due to the higher flexibility of the selected element, can  
268 result a bit overestimated. Consequently, stresses on the leaflets can result slightly lower (up to 10%),  
269 whereas the force exerted by the sutures does not experience any significant change.

270 The use of both more realistic geometric configuration and more physiologic boundary condition can  
271 further improve the results and highlight additional aspects of the NeoChord implant. It can be foreseen  
272 that, lastly, application of the presented approach to patient-specific anatomies may provide a useful tool  
273 for procedural planning, improving the efficacy of the treatment.

274 **CONCLUSIONS**

275 The present investigation compares the two most common tensioning procedures adopted in the  
276 transapical neochords implantation for mitral valve prolapse repair, i.e. ‘all together’ and ‘one by one’  
277 pulling approach. The study was performed on a generalized MV morphology, with prolapsed P2 scallop.  
278 Although idealized geometries and simplified constitutive behaviors were assumed, the study captures  
279 some of the clinical effects observed by surgeons, e.g. the unloading of previously pulled neochords.

280 The close similarity between healthy and repaired configuration obtained for all investigated strategies  
281 confirms the reliability and efficacy of the preferred surgical choice of four chords to treat the prolapse  
282 here considered.

283 Differences found in the results concerning coaptation area, stress distribution, and force on the neochords  
284 for AT and 1by1 repair suggest that the 1by1 lateral to central and lateral to lateral approaches are the  
285 most suitable solutions to reach maximum coaptation and maintaining operative leaflets stresses closer to  
286 those experienced in healthy conditions. AT strategy appears more conservative in terms of maximum  
287 stress during the intra-operative insertions since all the chords are activated at the same time, though this  
288 happens at the expense of the optimal valve closure.

289 Though this first study was based on a generalized symmetrical model, the robustness and reduced  
290 computational cost of the presented methodological approach makes it is suitable to be adopted for the  
291 clinical planning of the treatment in patient-specific cases. In addition, this model can represent the first  
292 step towards a more sophisticated platform, using patient-specific images to optimize the surgical  
293 procedure.

294 **Acknowledgments**

295 Authors thank Fondazione Cariparo, Padova, Italy, for funding Ph.D. fellowship of Luigi Di Micco. The  
296 Fondazione Cariparo had no involvement in the study design, in the collection, analysis, and interpretation  
297 of data, in the writing of the manuscript, and in the decision to submit the manuscript for publication.

298 This research has been also partially supported by the Fondazione Ing. Aldo Gini, Padova, Italy.

299 **Declarations**

300 *Competing interests:* None of the authors has any relationship with industry or financial associations that  
301 might pose a conflict of interest in connection with this work.

302 *Funding:* Fondazione Cariparo, Padova, Italy and Fondazione Ing. Aldo Gini, Padova, Italy.

303 *Ethical approval:* Not required.

304

305 **REFERENCES**

- 306 [1] G. Biglino, C. Capelli, J. Bruse, G. M. Bosi, A. M. Taylor, and S. Schievano, "Computational modelling  
307 for congenital heart disease: How far are we from clinical translation?," *Heart*, vol. 103, no. 2, pp.  
308 98–103, 2017.
- 309 [2] R. Toninato, J. Salmon, F. M. Susin, A. Ducci, and G. Burriesci, "Physiological vortices in the sinuses of  
310 Valsalva: An in vitro approach for bio-prosthetic valves," *J. Biomech.*, vol. 49, no. 13, pp. 2635–2643,  
311 2016.
- 312 [3] G. Burriesci, P. Peruzzo, F. M. Susin, G. Tarantini, and A. Colli, "In vitro hemodynamic testing of  
313 Amplatzer plugs for paravalvular leak occlusion after transcatheter aortic valve implantation," *Int. J.*  
314 *Cardiol.*, vol. 203, pp. 1093–1099, 2016.
- 315 [4] E. Votta *et al.*, "Toward patient-specific simulations of cardiac valves: State-of-the-art and future  
316 directions," *J. Biomech.*, vol. 46, no. 2, pp. 217–228, 2013.
- 317 [5] F. M. Susin, V. Tarzia, T. Bottio, V. Pengo, A. Bagno, and G. Gerosa, "In-vitro detection of thrombotic  
318 formation on bileaflet mechanical heart valves.," *J. Heart Valve Dis.*, vol. 20, no. 4, pp. 378–386,  
319 2011.
- 320 [6] A. Choi, D. D. Mcpherson, and H. Kim, "Computational virtual evaluation of the effect of  
321 annuloplasty ring shape," *Int. j. numer. method. biomed. eng.*, vol. 02831, no. September, pp. 1–11,  
322 2016.
- 323 [7] A. F. Members *et al.*, "Guidelines on the management of valvular heart disease (version 2012) The  
324 Joint Task Force on the Management of Valvular Heart Disease of the European Society of  
325 Cardiology (ESC) and the European Association for Cardio-Thoracic Surgery (EACTS)," *Eur. Heart J.*,  
326 vol. 33, no. 19, pp. 2451–2496, 2012.
- 327 [8] R. A. Nishimura *et al.*, "2014 AHA/ACC guideline for the management of patients with valvular heart  
328 disease," *Circulation*, p. CIR--0000000000000031, 2014.

- 329 [9] J. G. Castillo, J. Solís, Á. González-Pinto, and D. H. Adams, "Surgical Echocardiography of the Mitral  
330 Valve," *Rev. Española Cardiol. (English Ed.)*, vol. 64, no. 12, pp. 1169–1181, 2011.
- 331 [10] A. Colli, E. Bizzotto, D. Pittarello, and G. Gerosa, "Beating heart mitral valve repair with neochordae  
332 implantation: Real-time monitoring of haemodynamic recovery," *Eur. J. Cardio-thoracic Surg.*, vol.  
333 52, no. 5, pp. 991–992, 2017.
- 334 [11] A. Colli, R. Bellu, D. Pittarello, and G. Gerosa, "Transapical off-pump Neochord implantation on  
335 bileaflet prolapse to treat severe mitral regurgitation," *Interact. Cardiovasc. Thorac. Surg.*, p. ivv192,  
336 2015.
- 337 [12] A. Colli *et al.*, "Acute safety and efficacy of the NeoChord procedure," *Interact. Cardiovasc. Thorac.*  
338 *Surg.*, vol. 20, no. 5, pp. 575–581, 2015.
- 339 [13] P. Bajona, K. J. Zehr, J. Liao, and G. Speziali, "Tension Measurement of Artificial Chordae Tendinae  
340 Implanted Between the Anterior Mitral Valve Leaflet and the Left Ventricular Apex An In Vitro  
341 Study," vol. 3, no. 1, pp. 33–37, 2008.
- 342 [14] P. Bajona, W. E. Katz, R. C. Daly, K. J. Zehr, and G. Speziali, "Beating-heart, off-pump mitral valve  
343 repair by implantation of artificial chordae tendineae: An acute in vivo animal study," *J. Thorac.*  
344 *Cardiovasc. Surg.*, vol. 137, no. 1, pp. 188–193, 2009.
- 345 [15] H. Jensen *et al.*, "Transapical neochord implantation: Is tension of artificial chordae tendineae  
346 dependent on the insertion site?," *J. Thorac. Cardiovasc. Surg.*, vol. 148, no. 1, pp. 138–143, 2014.
- 347 [16] M. S. Reimink, K. S. Kunzelman, E. D. Verrier, and R. P. Cochran, "The Effect of Anterior Chordal  
348 Replacement on Mitral Valve Function and Stresses: A Finite Element Study.," *Asaio J.*, vol. 41, no. 3,  
349 pp. M754--M762, 1995.
- 350 [17] Y. Rim, S. T. Laing, D. D. McPherson, and H. Kim, "Mitral Valve Repair Using ePTFE Sutures for  
351 Ruptured Mitral Chordae Tendineae : A Computational Simulation Study," *Ann. Biomed. Eng.*, vol.  
352 42, no. 1, pp. 139–148, 2014.

- 353 [18] F. Sturla *et al.*, “Biomechanical drawbacks of different techniques of mitral neochordal implantation:  
354 When an apparently optimal repair can fail,” *J. Thorac. Cardiovasc. Surg.*, vol. 150, no. 5, pp. 1303–  
355 1312, 2015.
- 356 [19] A. E. Morgan, J. L. Pantoja, E. A. Grossi, L. Ge, J. W. Weinsaft, and M. B. Ratcliffe, “Neochord  
357 placement versus triangular resection in mitral valve repair: A finite element model,” *J. Surg. Res.*,  
358 vol. 206, no. 1, pp. 98–105, 2016.
- 359 [20] G. Gaidulis, E. Votta, M. Selmi, and S. Aidietien, “Numerical simulation of transapical off-pump mitral  
360 valve repair with neochordae implantation,” *Technol. Heal. Care*, vol. 26, 2018.
- 361 [21] K. D. Lau, V. Diaz, P. Scambler, and G. Burriesci, “Medical Engineering & Physics Mitral valve  
362 dynamics in structural and fluid – structure interaction models,” *Med. Eng. Phys.*, vol. 32, no. 9, pp.  
363 1057–1064, 2010.
- 364 [22] K. S. Kunzelman, D. R. Einstein, and R. P. Cochran, “Fluid-structure interaction models of the mitral  
365 valve: Function in normal and pathological states,” *Philos. Trans. R. Soc. B Biol. Sci.*, vol. 362, no.  
366 1484, pp. 1393–1406, 2007.
- 367 [23] A. Avanzini, G. Donzella, and L. Libretti, “Functional and structural effects of percutaneous edge-to-  
368 edge double-orifice repair under cardiac cycle in comparison with suture repair,” *Proc. Inst. Mech.  
369 Eng. Part H J. Eng. Med.*, vol. 225, no. 10, pp. 959–971, 2011.
- 370 [24] A. Avanzini, “A Computational Procedure for Prediction of Structural Effects of Edge-to-Edge Repair  
371 on Mitral Valve,” *J. Biomech. Eng.*, vol. 130, no. 3, p. 031015, 2008.
- 372 [25] F. Dal Pan, G. Donzella, C. Fucci, and M. Schreiber, “Structural effects of an innovative surgical  
373 technique to repair heart valve defects,” *J. Biomech.*, vol. 38, no. 12, pp. 2460–2471, 2005.
- 374 [26] B. Prescott, C. J. Abunassar, K. P. Baxevanakis, and L. Zhao, “Computational evaluation of mitral  
375 valve repair with MitraClip,” *Vessel Plus*, vol. 2019, pp. 0–10, 2019.
- 376 [27] K. May-Newman and F. C. Yin, “Biaxial mechanical behavior of excised porcine mitral valve leaflets,”

- 377 *Am. J. Physiol. Circ. Physiol.*, vol. 269, no. 4, pp. H1319--H1327, 1995.
- 378 [28] K. Kunzelman, M. S. Reimink, E. D. Verrier, R. P. Cochran, and R. W. M. Frater, "Replacement of  
379 Mitral Valve Posterior Chordae Tendineae with Expanded Polytetrafluoroethylene Suture: A Finite  
380 Element Study," *J. Card. Surg.*, vol. 11, no. 2, pp. 136–145, 1996.
- 381 [29] A. Colli *et al.*, "Transapical off-pump mitral valve repair with Neochord Implantation (TOP-MINI):  
382 step-by-step guide," *Ann. Cardiothorac. Surg.*, vol. 4, no. 3, p. 295, 2015.
- 383 [30] H. Muresian, "The clinical anatomy of the mitral valve," *Clinical Anatomy*, vol. 22, no. 1. pp. 85–98,  
384 2009.
- 385 [31] Y. Rim *et al.*, "Uncertainty quantification of inflow boundary condition and proximal arterial stiffness  
386 coupled effect on pulse wave propagation in a vascular network," *Ann. Biomed. Eng.*, vol. 9, no. 1,  
387 pp. 85–98, 2016.
- 388 [32] E. Votta, E. Caiani, F. Veronesi, M. Soncini, F. M. Montevocchi, and A. Redaelli, "Mitral valve finite-  
389 element modelling from ultrasound data: a pilot study for a new approach to understand mitral  
390 function and clinical scenarios," *Philos. Trans. R. Soc. A Math. Phys. Eng. Sci.*, vol. 366, no. 1879, pp.  
391 3411–3434, 2008.
- 392 [33] A. Colli *et al.*, "Prognostic impact of leaflet-to-annulus index in patients treated with transapical off-  
393 pump echo-guided mitral valve repair with NeoChord implantation," *Int. J. Cardiol.*, vol. 257, no.  
394 November 2015, pp. 235–237, 2018.
- 395 [34] A. Colli *et al.*, "Transapical off-pump mitral valve repair with Neochord implantation: Early clinical  
396 results," *Int. J. Cardiol.*, vol. 204, pp. 23–28, 2016.
- 397 [35] A. Colli *et al.*, "CT for the Transapical Off-Pump Mitral Valve Repair With Neochord Implantation  
398 Procedure," *JACC Cardiovasc. Imaging*, vol. 10, no. 11, pp. 1397–1400, 2017.

399

400 **FIGURES AND TABLES**

401 **Table 1.** Dimensional parameters adopted for leaflets and chordae of the MV model. Data were set in  
 402 accordance with [18] and [17]. APD and CD indicate the ateropostirial and commissures distance,  
 403 respectively.

<b>Leaflets</b>				
	<b>Anterior</b>	<b>Posterior</b>		<b>Commissure</b>
		<b>P2</b>	<b>P1/P3</b>	
<b>Height (mm)</b>	20	13.8	11.2	8.8
<b>Ann. Lenght (mm)</b>	32.3	17.5	12.7	6.7
<b>Area (mm<sup>2</sup>)</b>	457.6	204.4	123.9	51.2
<b>Thickness (mm)</b>	0.69	0.51		0.6
<b>Chordae Tendineae</b>				
<b>Cross-sectional area (mm<sup>2</sup>)</b>	0.29	0.27		0.28
<b>Annulus</b>				
<b>APD (mm)</b>	22			
<b>CD (mm)</b>	30			
<b>Area (mm<sup>2</sup>)</b>	552.7			

404

405 **Table 2.** Determined coefficients of equation (1) for anterior and posterior leaflets. (All units in MPa)

406

	<b>D<sub>1</sub></b>	<b>C<sub>10</sub></b>	<b>C<sub>20</sub></b>	<b>C<sub>30</sub></b>	<b>C<sub>40</sub></b>	<b>C<sub>50</sub></b>
<b>Anterior leaflet</b>	4.999	0.008	-0.073	0.742	-3.093	4.635
<b>Posterior leaflet</b>	6.564	0.006	0.001	0.015	-0.045	0.037

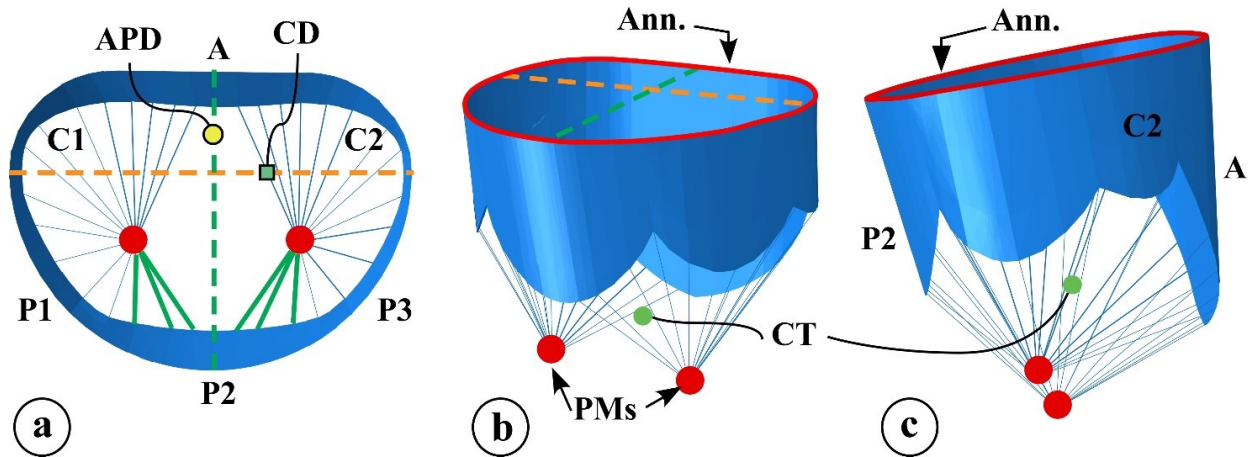
407

408 **Table 3.** Forces calculated on the neochords after the implantation of the four cases analyzed. Forces are  
 409 expressed in *N*

	<b>neochord</b>				<b>Tot</b>
	<b>a</b>	<b>b</b>	<b>c</b>	<b>d</b>	
<i>AT</i>	0.27	0.17	0.18	0.27	0.89
<i>Iby1a</i>	0.34	0.10	0.20	0.28	0.92
<i>Iby1b</i>	0.32	0.11	0.19	0.28	0.90
<i>Iby1c</i>	0.32	0.11	0.19	0.29	0.91

410

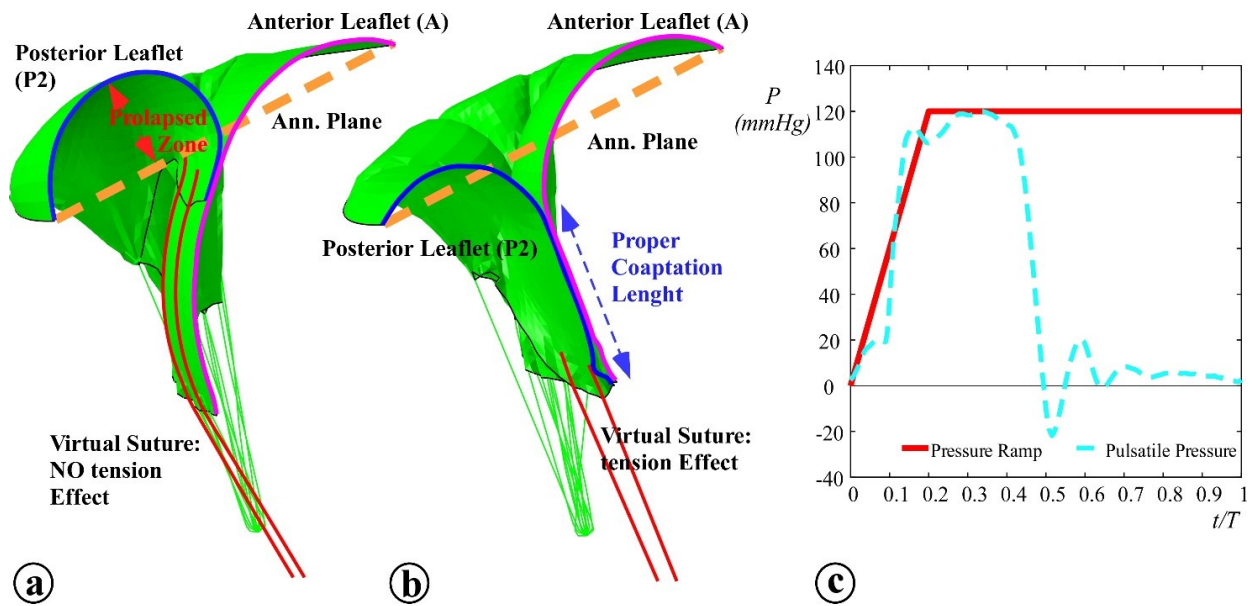
411



412

413 **Figure 1.** MV geometry of the model at the end of diastole. **a)** Atrial to ventricle view: A indicates the  
 414 anterior leaflet, C1 and C2 the commissural leaflet scallops, P1, P2 and P3 the posterior leaflet scallops, and  
 415 APD and CD the ateropostirial and commissures distance, respectively. **b)** Perspective view: red lines  
 416 indicates MV annulus. CT the chordae thendinae, and PMs the papillary muscles. **c)** Lateral view. The  
 417 chordae thendinae in green have been cut off to generate prolapse.

418

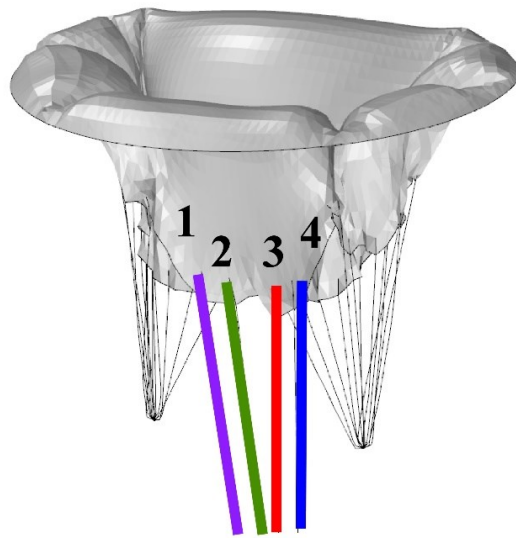


419

420 **Figure 2.** Restoration of MV. **a)** P2 prolapse before the tensioning of neochords (red lines). **b)** P2 prolapse  
 421 mitigation due to the tensioning of the neochords. Virtual sutures are inserted 3 mm far from leaflet free  
 422 margin. The contact line between anterior (magenta line) and posterior (blue line) leaflet determines the  
 423 coaptation length. **c)** Comparison between pulsatile (dotted line) and steady pressure condition (solid line)  
 424 linearly reached. The latter was applied to the ventricular surface of the valve for all simulation.

425

426

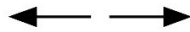


**All together strategy (AT)**

$$1 = 2 = 3 = 4$$

**One by one strategies (1by1)**

*a) Central to Lateral: 2;3;4;1*



*b) Lateral to Central: 1;4;2;3*



*c) Lateral to Lateral: 1;2;3;4*

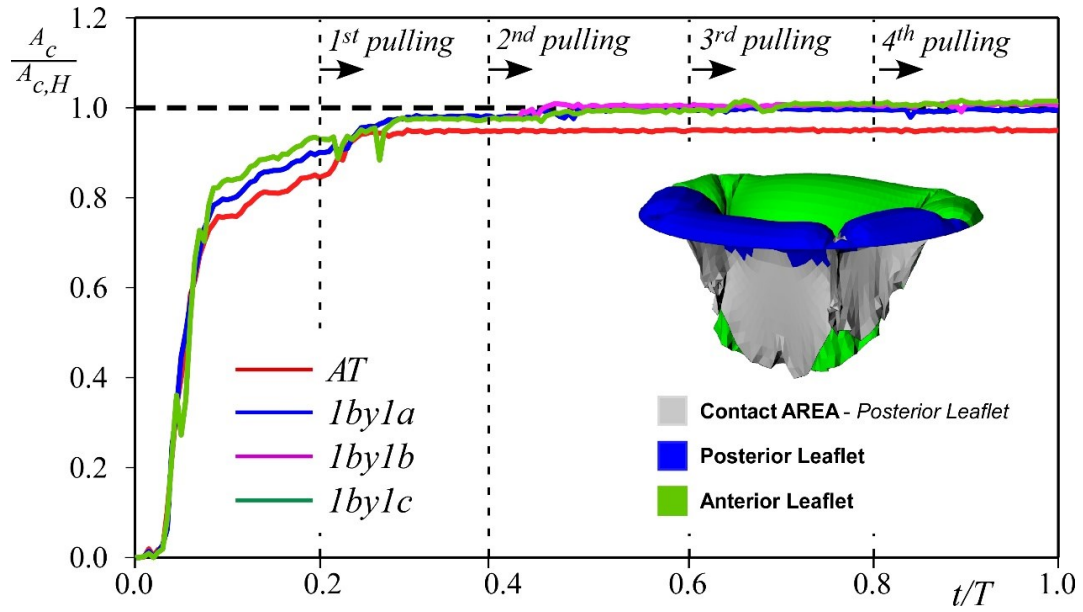


427

428 **Figure 3.** Simulated protocol tensiometer. In AT procedure all neochords are pulled together. In 1by1  
 429 procedure the chords are pulled one by one following three sequences: *a) central to lateral*, *b) lateral to*  
 430 *central*, and *c) lateral to lateral*. In all simulations, neochords are numbered in crescent order starting from  
 431 left external position to right external position.

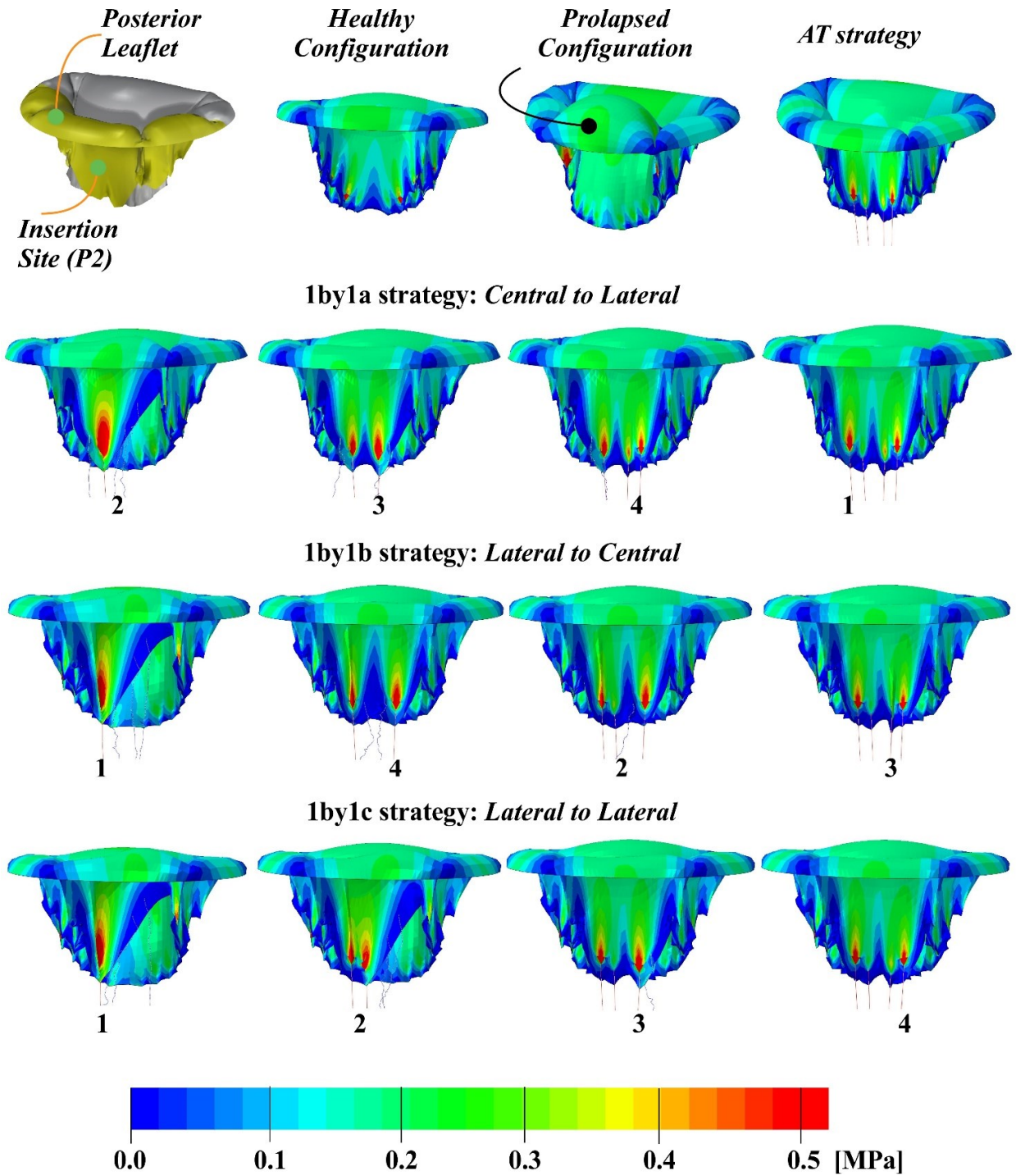
432

433



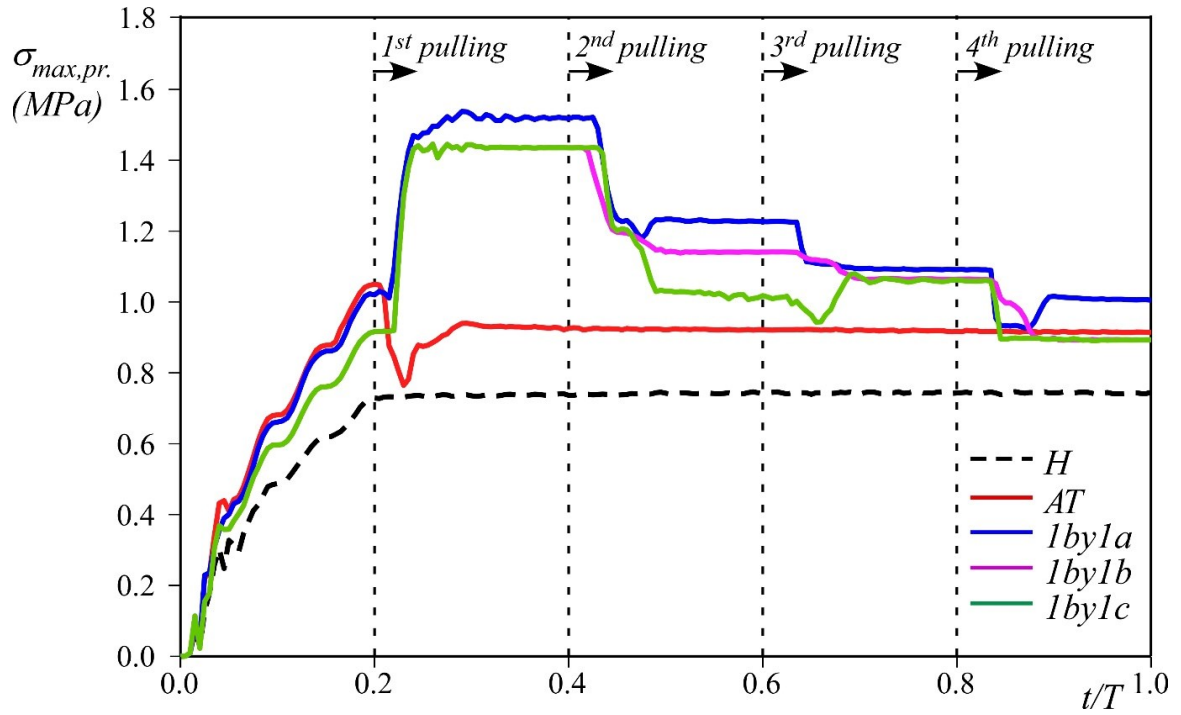
434

435 **Figure 4.** Overall contact area on the Posterior leaflet during chord tensioning normalized with the contact  
 436 area of the healthy configuration  $A_{c,H}$ . Red line represents *AT strategy*, blue, magenta and green lines  
 437 represent *lby1 strategies* following sequence *a)*, *b)* and *c)* of Figure 3, respectively.



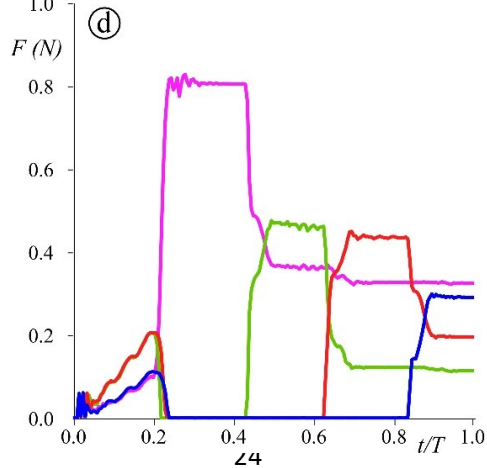
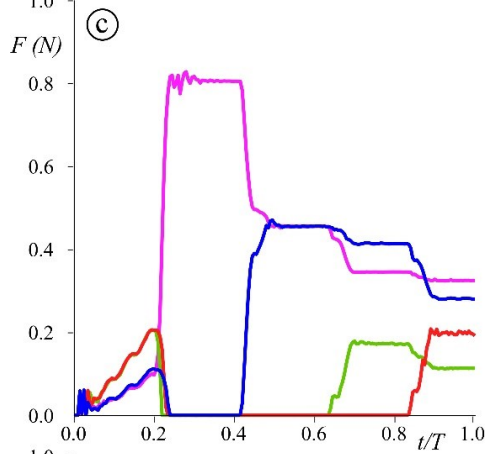
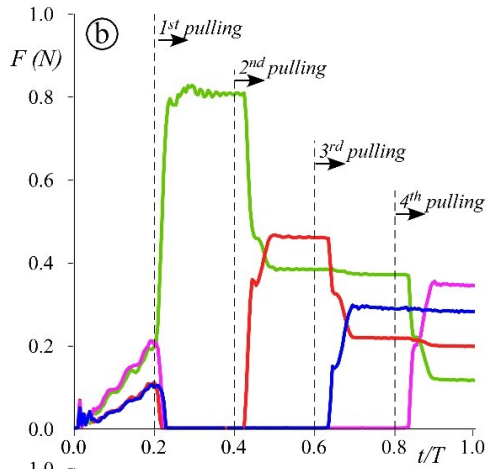
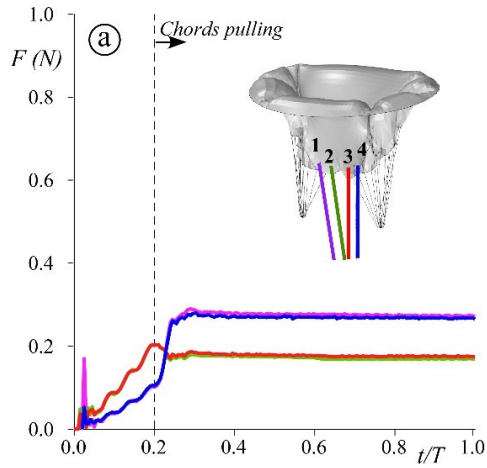
439

440 **Figure 5.** MV stress patterns at systolic peak. Leaflet stress in *healthy configuration*, *prolapsed configuration*  
 441 with inactive neochords, *AT strategy* configuration, and *1by1 strategy* at different steps of pulling. The  
 442 stress field in 1by1 cases is reported after the complete load of the neochord labeled by the irrespective  
 443 number.



445

446 **Figure 6.** Maximum principal stress calculated on the P2 scallop during simulations. The black dotted line  
 447 represents the stress calculated for the Healthy configuration ( $H$ ). The red line represents the AT strategy.  
 448 The blue, magenta and green lines represent 1by1 strategies following sequence a), b) and c) of Figure 3,  
 449 respectively.



451 **Figure 7.** Force applied by neochords during the implant in **a)** *AT strategy*, **b)** *1by1a (central to lateral*  
452 *sequence)*, **c)** *1by1b (lateral to central sequence)*, and **d)** *1by1c (lateral to lateral sequence)*.